

THE GAS-PHASE DERIVATIZATION OF COAL

A.W. Wells, R.F. Frank, and K. Waldner

U.S. Department of Energy
Pittsburgh Energy Technology Center
Pittsburgh, Pennsylvania 15236

Introduction

Most of the spectroscopies employed to study reactive functionalities on the surface of coal suffer because a high percentage of adsorption from bulk or subsurface functional groups are included. For example, photoacoustic infrared Fourier transform (PAIFT) spectroscopy, while one of the most surface selective of the infrared spectroscopies, still has a thermal diffusion length of approximately 20 micrometers for a coal particle of 150 micrometers radius under typical experimental conditions.¹ Spectroscopic techniques are also limited in their ability to provide accurate quantification due to difficulties in estimating adsorption coefficients and the need to employ such techniques as curve deconvolution.

An alternative approach is to employ a probe molecule that will interact with reactive functional groups on the surface of coal and to quantify the degree of interaction. Although this approach is in its infancy, some success has been demonstrated for flow microcalorimetry using acidic and basic probes.^{2,3,4} A logical extension to this approach would be to employ probe molecules that react with specific surface functionalities to form products that can be accurately quantified without the use of surface spectroscopies. Information on total surface functionality content should also provide complementary information to surface functionality densities obtained from spectroscopies such as X-ray photoelectron spectroscopy.^{5,6} It was the purpose of this investigation to test the feasibility of this approach using the gas-solid phase silylation of hydroxyl groups on coal with hexamethyldisilazane (HMDS) in nitrogen.

The kinetics of the chemisorption of HMDS vapors into 100-mesh Illinois No. 6 coal particles were followed by periodic removal from the reactor of portions of the coal. The coal was subsequently analyzed for its trimethylsilyl ether content. The kinetics were evaluated using a mathematical model applied by Berens and Hopfenberg to describe the sorption of vinyl chloride monomer, acetone, and methanol vapors into powder samples of polyvinyl chloride.⁷ For experiments in which "glassy" polymers were continuously exposed to relatively large concentrations of sorbate, a striking two-phase sorption process was observed by News⁸ and by Long and Richman.⁹ The two stages were separated in time and consisted of an initial, rapid Fickian diffusion process that was followed by a much slower relaxation process. Berens and Hopfenberg interpreted the diffusion process as involving migration of penetrant molecules into preexisting void space, and the relaxation process as related to swelling, resulting from large-scale segmental motions of the polymer.⁷

These preliminary investigations attempted to exploit the two-stage sorption kinetics to define reaction parameters that would result in a high level of surface selectivity while minimizing relaxation and swelling of the bulk of the coal's macromolecular structure. The effects of particle size were evaluated by Enscoe et al.¹⁰ who demonstrated that under proper conditions of temperature and penetrant activity, n-hexane sorption into about 200 micrometer diameter polystyrene spheres was dominated by a relaxation mechanism whereas sorption into submicron polystyrene spheres was predominantly by way of Fickian diffusion. As suggested by Vrentas et al.,¹¹ the relaxation process is independent of the particle size of the polymer but the Fickian diffusion time frame varies with the square of the particle size. Two-stage behavior, therefore, can be approached by increasing the diffusion rate through increased reagent activity and by reducing the diffusive path length by decreasing the particle size. Ideally, the Fickian diffusion coefficient should be at least an order of magnitude greater than the first-order relaxation rate constant for the predominant relaxation mode.

A corollary consideration in designing experiments to elicit two-stage behavior would be to reduce the relaxation rate by selecting penetrants with a low solubility in the polymer. Ritgar and Peppas¹² modeled the sorption of pyridine vapors by thin films of bituminous coals using the Berens and Hopfenberg equation and found that the process could be modeled using a single first-order relaxation term. The relaxation rate constant remained nearly the same over a range of coal carbon content and sample thickness, indicating the process to be mechanistically characteristic of the penetrant. The relatively rapid relaxation of coal by pyridine vapor would presumably make it difficult to construct experimental conditions where two-phase behavior would be observed. Two-phase behavior was observed by Hsieh and Duda for the sorption of toluene vapor by pyridine extracted bituminous coal powders.¹³ The removal of the "mobile phase" in coal by pyridine extraction decreased penetrant uptake. Hsieh and Duda also observed an initial rapid adsorption onto the surface of the coal particles.¹³ These observations of two-stage behavior suggest an approach to obtaining surface selectivity. HMDS was selected as a suitable vapor phase chemisorption probe, in part, because of a low solubility in bituminous coals.

The Berens and Hopfenberg model is a linear combination of a Fickian diffusion component and of one or more first-order relaxation components.

$$M_t = M_\infty \left\{ 1 - \frac{6}{\pi^2} \sum_{n=1}^{\infty} \frac{1}{n^2} \exp(-n^2 k_r t) \right\} + \sum_i M_{s,i} \left[1 - \exp(-k_{s,i} t) \right]$$

Where: M_t is the total sorption due to Fickian diffusion,
 $M_{x,i}$ is the total sorption due to the i th relaxation mode,
 M_t is the total sorption at time t ,
 k , is the Fickian rate constant, and
 $k_{x,i}$ is the first-order rate constant for the i th relaxation mode.

The relaxation components in this model are driven by the release of stresses within the polymeric macromolecule through penetrant-induced swelling. The relaxation processes are, unlike Fickian diffusion, unrelated to particle size.

Experimental

The gas-solid phase silylation reactions were carried out in a 250-mL, three-necked, round-bottom, nitrogen-flushed flask. For kinetic studies, coal samples were periodically removed from the reactor through an "entrance port" fitting. The fitting directly above the coal sample was used for reagent addition. This fitting supported a Mininert valve above the reactor and a 1 mL, "evaporation" beaker which could be heated by being lowered against the bottom interior of the reaction flask. A glass capillary tube connected the Mininert valve to the evaporation beaker. The capillary tube could be raised or lowered through an O-ring fitting. The bottom of the flask was placed into a heating mantle and the temperature was monitored using a thermocouple. All fittings were Teflon with Viton O-ring seals to avoid the use of sealants that might contaminate the surface of the coal particles.

The coal sample (0.8 g of Argonne premium Illinois No. 6 coal) was spread out on the bottom of the flask and the flask flushed with nitrogen. The reaction was initiated by addition of 500 microliters of HMDS, which was rapidly volatilized. Saturation with HMDS was maintained throughout the experiment. Approximately 70-mg coal samples were removed at various time intervals for analysis. Their trimethylsilyl ether content was determined after 3 hours of vacuum drying to remove physically adhering reagent. The trimethylsilyl ether content was determined using a fluoride cleavage-G.C. headspace procedure. Gas-solid-phase silylations were carried out at coal temperatures of 123, 163, 178, and 196 degrees C. Ten mL of a solution of 65% THF, 25% concentrated HF, and 10% water (by volume) were used to cleave the trimethylsilyl ethers in a 30-mL Teflon test tube fitted with a Mininert cap, valve, and septum assembly. The reaction was carried out at room temperature. In the reaction, hydrofluoric acid cleaves the trimethylsilyl ethers, converting them into trimethylfluorosilane, which is largely soluble in the reaction solution. The coal-hydroxyl groups are regenerated in the process. One-half milliliter of headspace was sampled and analyzed for trimethylfluorosilane on a Poropak P column maintained isothermally at 185°C. The trimethylfluorosilane peak area was calibrated against a standard curve generated by fluoride cleavage of various amounts of the TMS ether of 1-naphthol (Figure 1). As shown in Figure 1, deviations from Henry's law (linearity) begin at 20 microliters of standard. Sample weights were adjusted to utilize the linear range of the standard curve. The TMS ether of 1-naphthol was obtained by refluxing 1-naphthol in a 1:1:2.5 mixture of HMDS:TMCS:Pyridine, and distilling the crude product at 90 -91°C under 1 mm of nitrogen.

Results and Discussion

The Berens and Hopfenberg model was modified slightly by the addition of a separate term, M_1 , to describe a rapid, initial chemisorption occurring within the first few minutes and presumably resulting from the unimpeded contact of reagent vapors with the surface of larger pores. The computer-assisted curve fitting process for obtaining equation parameters was essentially the same as that described by Berens and Hopfenberg.⁷ A computer program was used to minimize the summed-squares deviations between measured values and the corresponding values generated from the equation by adjusting the constants.

A comparison between the equation and measurements obtained at 178°C is shown in Figure 2 together with curves representing contributions from individual terms of the equation. Two-stage behavior was clearly evident for curves generated over the reaction temperature range of 123° to 196°C. Appropriate, early termination of the reaction would result in the initial and diffusion terms constituting an average of 89% of the total chemisorption. The time required to reach diffusion equilibrium was less at 196°C, 3 hours to reach 93% of maximum, than at lower temperatures where 6 hours were required to reach 93% of maximum. The total contributions at infinity for the two relaxation terms, M_{r_1} and M_{r_2} , for the Fickian diffusion term, M_f , and for the summation of terms, M_{total} , are given as a function of reaction temperature in Figure 3. The Fickian diffusion term plateaued at 178°C as did the principle relaxation mode, r_2 . The minor relaxation mode, r_1 , does not plateau over the temperature range.

While specific polymeric motions cannot be identified with r_1 or r_2 relaxations, a case can be made for a linkage between the diffusion term and r_2 relaxation (Figure 2.) Pore deformation and a corresponding expansion of the nascent void space might result from chemical modification of the pore surface, the disruption of intrapore hydrogen bonding, or from steric interactions as the pores are filled. Gethner⁸ utilized light scattering to probe changes in the larger pores of an Illinois No. 6 coal when immersed in each of 7 different liquids and concluded that such pores were not rigid but easily deformed. Void-structure alterations were clearly evident and resulted in an increase of the total void-volume contributing to the light scattering. Information on sorbate-induced polymeric rearrangements or conformational transformations associated with the relaxation of coal cannot be obtained directly from phenomenological measurements of sorbate uptake. Coal relaxation linked to solvent or vapor sorption is, however, invariably correlated to coal swelling. In the chemisorption of HMDS into Illinois No. 6 coal, a single relaxation term accounts for the majority of reagent uptake and is assumed to reflect the gradual 'opening' of the macromolecular coal networks. For gas-phase, surface-limited applications, however, the silylation is terminated before appreciable polymeric relaxation and corresponding penetration of the coal matrix has occurred. This should presumably reduce opportunities for matrix entrapment of reagent.

The kinetic studies were used to define 'standard' conditions for surface-limited derivatizations of 178°C and a 6 hour reaction time. Ten replicate determinations under these conditions gave a total surface hydroxyl content of 0.76 hydroxyl groups / 100 carbon atoms with a standard deviation of 0.02 hydroxyl groups / 100 carbon atoms. This compares with a total hydroxyl content for Illinois No. 6 premium coal of 4.7 hydroxyl groups / 100 carbon atoms determined from liquid phase silylation reactions. This technique could be very

useful in following changes in coal surface chemistry when the surface is subjected to modification.

While the concept of coal surface is defined through the choice of experimental conditions and probe, an approach based upon limiting relaxation of the coal structure is reasonable. In contrast to spectroscopies, molecular probes should access the surface of pore systems where much of the liquid-solid and gas-solid interfacial chemistry of coal processing technologies occur. The gas-solid phase derivatization approach to coal surface analysis should result in an improved ability to quantify surface functionality content and to obtain a greater level of chemical selectivity through functionality specific reactions.

References

1. T. Zerlita *Applied Spectroscopy* 1986, 40, 214.
2. F.M. Fowkes, K.L. Jones, L. Guozhen, and T.B. Lloyd *Prepr. Pap. - Am. Chem. Soc., Div. Fuel Chem.* 1987, 32(1), 216.
3. D.W. Fuerstenau, G.C. Yang, and S. Chander *Prepr. Pap. - Am. Soc., Div. Fuel Chem.* 1987, 32(1), 209.
4. D. Brooks, A. Finch, P.J. Gardner, and R. Harington *Fuel* 1986, 65, 1750.
5. D.L. Perry and A. Grint *Fuel* 1983, 62, 1024.
6. D.T. Clark and R. Wilson *Fuel* 1983, 62, 1034.
7. A.R. Berens and H.B. Hopfenberg *Polymer*, 1978, 19, 489.
8. A.C. Newns *Trans. Faraday Soc.* 1956, 52, 1533. (Ref. 9(12))
9. F.A. Long and D. Richman *J. Am. Chem. Soc.* 1960, 82, 513. (Ref. 7(14))
10.D.J. Ensore, H.B. Hopfenberg, and V.T. Stannett *Polymer* 1977, 18, 793. (Ref. 7(8))
11. J.S. Vrentas, C.M. Jarzebski, and J.L. Duda *AIChE J.* 1975, 21, 894. (Ref. 7(7))
12. P.L. Ritger and N.A. Peppas *Fuel* 1987, 66, 1379.
13. S.T. Hsieh and J.L. Duda *Fuel* 1987, 66, 170.
14. J.S. Gethner *Prepr. Pap. - Am. Chem. Soc., Div. Fuel Chem.* 1987, 32(1), 239.
15. H. Marsh *Carbon* 1987, 25(1), 49.

FIGURE 1

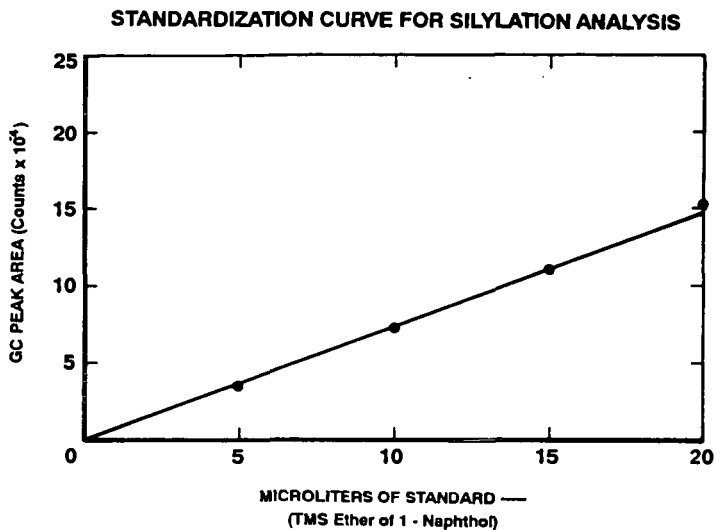


FIGURE 2

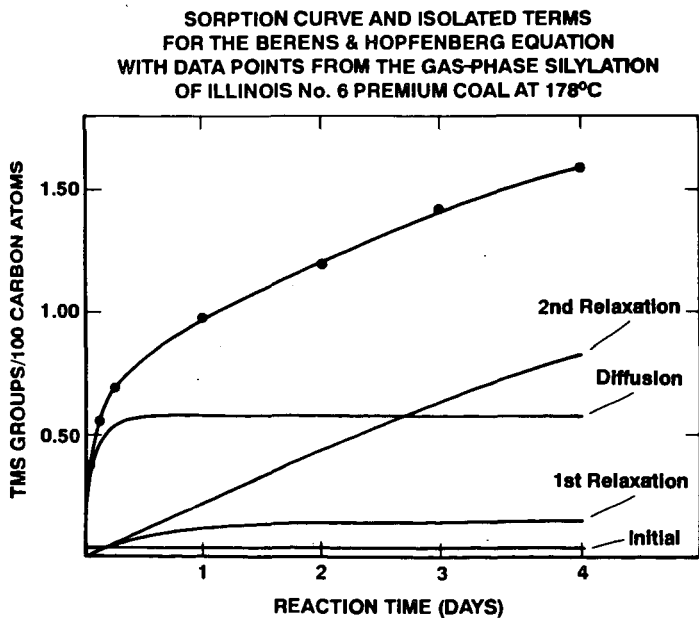
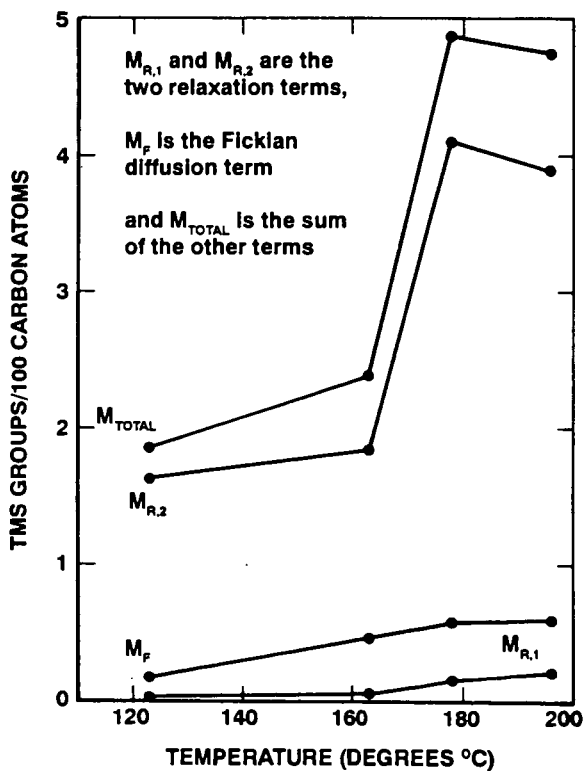


FIGURE 3

TEMPERATURE PROFILE OF TERMS
 FROM THE BERENS & HOPFENBERG EQUATION
 AT INFINITY FOR THE GAS-PHASE SILYLATION
 OF ILLINOIS No. 6 PREMIUM COAL



**LASER DESORPTION ION TRAP MASS SPECTROMETRY
OF THE MACROMOLECULAR COMPONENT OF COAL**

John A. Burroughs, Brian M. Cadre, and Luke Hanley
University of Illinois at Chicago
Department of Chemistry, m/c 111
Chicago, IL 60607-7061

Keywords: coal, laser desorption, mass spectrometry

INTRODUCTION

The structure of coal has been proposed to be a macromolecular network in which smaller molecules are confined [1]. It follows that a portion of the organic sulfur and other heteroatoms present in coal are covalently bound to this network. This paper describes efforts to measure high molecular weight mass spectra representative of this macromolecular network and ultimately, determine the chemical structure of organic sulfur contained therein.

Indirect evidence for the existence of a two component coal structure has been provided by solvent swelling, nuclear magnetic resonance, and various other measurements [1,2]. Size exclusion chromatography (SEC) has been used to determine that the number average molecular weight (M_n) of polymers extracted from coal with pyridine and other solvents ranges from 1000 to above 10,000 amu [3-5]. However, SEC experiments on coal polymers are limited by the difficulty in calibrating the retention time of what are essentially unknown chemical compounds. Thus, M_n values obtained by SEC differ by ~20% from values obtained with vapor phase osmometry [4]. Furthermore, only the soluble portion of the coal sample is analyzed by these methods and SEC has not provided a detailed chemical description of these coal polymers. Mass spectrometry is a logical method for measuring M_n of coal polymers. Nevertheless, experiments which have utilized ion bombardment [6], pyrolysis [7,8], electric field gradients [9], or pulsed lasers [10-12] for desorption and ionization of coal polymers have only formed low molecular weight ions via thermal degradation and chemical transformation rather than intact, high molecular weight ions.

The experiments described here attempt to exploit recent advances in high molecular weight mass spectrometry to generate representative ions of coal polymers. Infrared and ultraviolet laser desorption methods are applied to pyridine solvent extracts of high sulfur coals, where any ions formed are detected by an ion trap mass spectrometer. Ion trap mass spectrometers can measure the mass to charge (m/z) ratio of ions over a wide mass range, can perform collision induced dissociation experiments for structural analysis of ions, and can be operated in a high resolution mode [13].

EXPERIMENTAL DETAILS

A schematic diagram of the experimental apparatus is shown in Figure 1. To obtain a mass spectrum up to ~650 m/z , ions formed by laser desorption from a coal sample are injected through holes in the end cap of the ion trap into its center [13]. The ions are contained

inside the trap by an initial radio frequency voltage applied to the ring electrode while the end cap electrodes are held at ground potential. After the ions have undergone many collisions with a helium buffer gas, the radio frequency amplitude is ramped linearly, causing ions of increasing m/z values to be ejected from the trap through holes in the end caps. The ions which exit the ion trap are detected by a conversion dynode/channeltron ion detector.

The mass range of the ion trap is extended via the application of an auxiliary frequency across the end cap electrodes concurrent with the rf amplitude ramp. Ions up to 10,000 m/z have been detected with this apparatus to date and future experiments should extend this towards the theoretical limit of ~40,000 m/z . Trapping of individual mass ions has also been accomplished, as a predecessor to collision induced dissociation experiments.

The ion trap mass spectrometer was constructed by mounting the electrodes from an commercially available ion trap detector (Finnigan MAT ITD 700) inside a diffusion pumped vacuum chamber with a base pressure of $\sim 2 \times 10^{-8}$ Torr. A 6 kV conversion dynode is located adjacent to the channeltron near the exit end cap electrode to allow for high mass detection. Roughly 10^{-3} Torr of helium buffer gas is introduced into the trap via a leak valve. Experimental timing sequences and data acquisition are controlled with an IBM compatible 80386 microcomputer interfaced to the commercial ion trap electronics via plug-in multifunction data acquisition boards (National Instruments models AT-MIO-16F-5 and PC-TIO-10). The end cap electrodes are connected to a function generator (Stanford Research Systems DS345) through a homemade buffer amplifier.

To perform infrared laser desorption experiments, pulses of 1064 nm radiation of ~7 ns duration from a Nd:YAG laser (Continuum Surelite) are focussed onto the sample probe resulting in power densities of 10^9 - 10^{10} W/cm². The power density is calculated by visual estimation of the laser spot diameter on the sample probe tip and by measuring the unfocussed laser power with a pyroelectric joulemeter (Molelectron). For ultraviolet laser desorption, fourth harmonic generation of the Nd:YAG fundamental wavelength gives 266 nm pulses in the 10^9 - 10^{10} W/cm² power density range.

Solvent extracts from coal are prepared by dissolving powdered coal in pyridine and allowing the samples to equilibrate for three days at room temperature, then filtering out the insoluble portion which remains. Experiments were performed using Pocahontas No. 3 and Illinois No. 6 coal from the Argonne Premium Coal Sample Program and Herrin No. 6 (IBC 101) coal from the Illinois Basin Coal Sample Program.

RESULTS AND DISCUSSION

Laser desorption MS using infrared radiation has been used for the analysis of various nonvolatile organic molecules, biomolecules, and synthetic polymers [14]. The technique usually involves irradiating the sample at power densities from 10^7 - 10^{10} W/cm². In many cases the sample is doped with an inorganic salt to assist the formation of cation-attached molecular ions. Here, infrared laser

desorption was used to generate spectra from a series of poly(ethyleneglycol) standards of known molecular weight (American Polymer Standards) doped with KCl. Cation-attached molecular ions up to $\sim 10,000$ m/z were successfully formed and detected using this method.

Laser desorption experiments utilizing infrared radiation to desorb and ionize either disburbed solid coal or solvent extracts of same have been unsuccessful in generating any meaningful information regarding the macromolecular structure of coal. The only observable peaks above ~ 300 m/z in these spectra were due to the presence of carbon cluster ions, as verified by comparison with similar clusters formed in laser desorption of graphite samples. Attempts to dope the coal samples with KCl, NaCl, and CsCl to enhance the formation of cation attached ions have all failed to produce intact molecular ions. It is concluded that regardless of the sample preparation method, infrared laser desorption of coal and coal extracts is not a useful method for generating the desired high molecular weight ions, in agreement with previous experiments along these lines [10-12].

Ultraviolet matrix assisted laser desorption/ionization (UVMALDI) has recently emerged as a useful tool for forming intact molecular ions up to $300,000$ m/z of various biopolymers including proteins and carbohydrates as well as synthetic polymers [15-17]. The technique requires that the analyte molecule, usually exhibiting only moderate optical absorption at the desorption wavelength, be sparsely dispersed in a strongly absorbing matrix [15]. Much lower power densities (i.e. 10^6 - 10^7 W/cm²) are used in a typical UVMALDI experiment than with infrared laser desorption [18], but the former method is capable of desorbing intact far larger and more labile species than the latter. Although time-of-flight mass spectrometers are most often employed in such experiments, ion traps have been used to detect ions formed by UVMALDI [19-21].

The matrix which was used for both test compounds and for coal extract samples is 2,5-dihydroxybenzoic acid (DHB). For the first test sample, gramicidin S was dissolved in a water/ethanol solution in a 1000:1 molar mixture of matrix/analyte. A second test sample of bovine insulin was similarly prepared in a 5000:5000:1 DHB/d-fructose/bovine insulin mixture. Intact molecular ion peaks from gramicidin S (1140 m/z) and bovine insulin (5733 m/z) have been formed and detected with UVMALDI and the spectra for the later is shown in Figure 2; The intact molecular ion and the ionized chain B portion of the molecule are present, but no other fragments are observed.

Unfortunately, attempts to generate intact macromolecular ions from the pyridine soluble portion of various coals using the UVMALDI technique have not yet been successful. Detection of sample molecules using UVMALDI requires that the analyte molecule be capable of forming a stable ion in the gas phase, presumably by accepting or donating a proton or other cation. The various proposed structures of coal all contain numerous ionizable groups such as S or N-containing heterocyclic rings, hydroxides, or sulfides [22]. Therefore, it should be possible to produce intact molecular ions from coal using UVMALDI.

It is postulated that the failure of UVMALDI to generate intact ions from coal polymers derives from improper sample preparation. Preparing a proper sample of a new compound for UVMALDI is at present

a trial and error process in which matrix type, matrix-to-analyte ratio, and concentration of cation donating dopants are all varied [15,23]. Furthermore, while some samples produce positive ions, others generate only negative ions. To date, only positive ions have been sought in these experiments. New sample preparations and negative ion formation are presently under exploration. Therefore, a final conclusion cannot yet be drawn regarding the applicability of laser desorption ion trap mass spectrometry to the study of polymers from coal.

ACKNOWLEDGEMENTS

This work was prepared with the support, in part, by grants made possible by the Illinois Department of Energy and Natural Resources through its Coal Development Board and Illinois Clean Coal Institute, and by the U.S. Department of Energy (Contract Number DE-FG22-91PC91334). However, any opinions, findings, conclusions, or recommendations expressed herein are those of the authors and do not necessarily reflect the views of IDENR, ICCI, or DOE.

REFERENCES

- 1) P.H. Given, A. Marzec, W.A. Barton, L.J. Lynch, and B.C. Gerstein, *Fuel* **65** (1986) 155.
- 2) F. Derbyshire, A. Marzec, H.-R. Schulten, M.A. Wilson, A. Davis, P. Tekely, J.-J. Delpuech, A. Jurkiewicz, C.E. Bronnimann, R.A. Wind, G.E. Maciel, R. Narayan, K. Bartle, and C. Snape, *Fuel* **68** (1989) 1091.
- 3) J.L. Wong in "Coal Science and Chemistry", A. Volborth, ed., Elsevier (Amsterdam, 1987) 461.
- 4) D.H. Buchanan, L.C. Warfel, S. Bailey, and D. Lucas, *Energy Fuels* **2** (1988) 32.
- 5) J.W. Larsen and Y.-C. Wei, *Energy Fuels* **2** (1988) 344.
- 6) J.M. Lytle, G.L. Tingey, and R.D. Macfarlane, *Anal. Chem.* **54** (1982) 1881.
- 7) R.E. Winans and P.H. Neill, in "Geochemistry of Sulfur in Fossil Fuels", W.L. Orr and C.M. White, eds., ACS (Washington, 1990) 249.
- 8) P.J.J. Tromp, J.A. Moulijn, and J.J. Boon in "New Trends in Coal Science", Y. Yurum, ed., Kluwer Academic (Dordrecht, 1988) 241.
- 9) J.A.G. Drake, D.W. Jones, D.E. Games, and J.L. Gower, *Fuel* **63** (1984) 634.
- 10) J.E. Hunt, K.R. Lykke, and R.E. Winans, *Fuel Chem. Div. Am. Chem. Soc.* **36** (1991) 1325.
- 11) T. Mauney, *Anal. Chim. Acta* **195** (1987) 337.
- 12) P.F. Greenwood, M.G. Strachan, H.J. El-Nakat, G.D. Willett, M.A. Wilson, and M.I. Attalla, *Fuel* **69** (1990) 257.
- 13) R.G. Cooks, G.L. Glish, S.A. McLuckey, and R.E. Kaiser, *Chem. Eng. News* **69:12** (1992) 26.
- 14) R.B. Cody, A. Bjarnason, and D.A. Weil in "Lasers and Mass Spectrometry", D.M. Lubman, ed., Oxford University (New York, 1990) 316.
- 15) F. Hillenkamp, M. Karas, R.C. Beavis, and B.T. Chait, *Anal. Chem.* **63** (1991) 1193A.

- 16) U. Bahr, A. Deppe, M. Karas, F. Hillenkamp, and U. Giessmann, *Anal. Chem.* **64** (1992) 2866.
- 17) P.O. Danis, D.E. Karr, F. Mayer, A. Holle, and C.H. Watson, *Org. Mass Spectrom.* **27** (1992) 843.
- 18) B.U.R. Sundqvist, *Int. J. Mass Spectrom. Ion Proces.* **118/119** (1992) 265.
- 19) M.E. Bier, J.C. Schwartz, I. Jardine, and G. Stafford; *Proc. 40th ASMS Conf. Mass Spectrom. and Allied Topics*, Washington, DC, 31 May - 5 June 1992, 117.
- 20) D.M. Chambers, D.E. Goeringer, S.A. McLuckey, and G.L. Glish; *Proc. 40th ASMS Conf. Mass Spectrom. and Allied Topics*, Washington, DC, 31 May - 5 June 1992, 1747.
- 21) V. Doroshenko, T. Cornish, and R.J. Cotter; *Proc. 40th ASMS Conf. Mass Spectrom. and Allied Topics*, Washington, DC, 31 May - 5 June 1992, 1753.
- 22) G.A. Carlson and B. Granoff, in "Coal Science II", H.H. Schobert, K.D. Bartle, and L.J. Lynch eds., ACS (Washington, 1991) 159.
- 23) T-W.D. Chan, A.W. Colburn, P.J. Derrick, D.J. Gardiner, and M. Bowden, *Org. Mass Spectrom.* **27** (1992) 188.

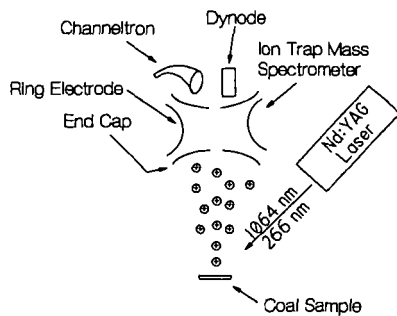


Figure 1: Schematic diagram of the laser desorption ion trap mass spectrometer.

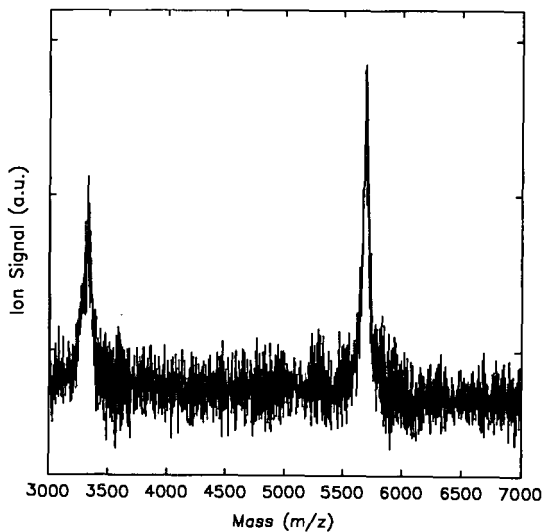


Figure 2: UVMALDI spectrum of a trial compound, bovine insulin, demonstrating the feasibility of the method for labile high molecular weight compounds such as coal polymers.

MEASUREMENT OF THE ADSORPTION AND CRACKING OF MODEL COMPOUNDS OVER PROCESSED OIL SHALE PARTICLES

Darrell N. Taulbee,
Center for Applied Energy Research,
3572 Iron Works Pike,
Lexington, KY 40511, (606) 257-0238

Keywords: Cracking reactions, adsorption-desorption, oil shale.

A parallel reactor system has been constructed to monitor adsorption, desorption, and/or cracking/coking of vapor phase model compounds over solid substrates at elevated temperatures. In this study, selected hydrocarbons ranging from benzene to n-decane were passed across pyrolyzed, gasified, or combusted oil shale particles at temperatures between 270 °C and 650 °C. A vapor phase hydrocarbon, Ar tracer gas, and N₂ carrier are combined and routed through a heated switching valve to a sand-packed tube reactor positioned within a tube furnace. A parallel line routes N₂ gas through a second tube reactor packed with substrate. After exiting the tube reactors, the two lines are combined and sampled by a heated capillary connected to the inlet of a quadrupole mass spectrometer (QMS). A typical run entails establishing a QMS baseline with the model compound passing through the sand-packed reactor, switching the valve so the model compound passes through the substrate bed, then returning to the sand-packed reactor to re-establish the QMS baseline.

Introduction. The utilization of fluidized bed retorting technology for the processing of the Eastern US oil shale deposits has been under investigation at the CAER since about 1982. Development has progressed from small independent grams/hours pyrolysis, combustion, and gasification reactors, through operation of an integrated, 3-stage, 5-lb/hr unit and currently, construction of an integrated 50-lb/hr pilot plant representing the most recent effort to provide proof of concept for KENTORT II. KENTORT II is designed to maximize oil and gas production and to fully utilize the carbon contained in Eastern US oil shales without resorting to exotic or high pressure atmospheres^{1,2} and to do so in an environmentally acceptable manner.

In the KENTORT II reactor, pyrolysis heat is provided by recycling hot gasified or combusted particles to the pyrolysis zone. Thus, of particular interest are those reactions that can be attributed to the recycling of hot solids and which impact oil yield, i.e., cracking and coking reactions. Within limits, the detrimental effect of recycling hot solids to the retort can be minimized by varying the relative proportion of gasified versus combusted particles or by selecting the optimum recycle rate/particle temperature, i.e., fewer high temperature vs. more low temperature particles.

A previous study³⁻⁴ focused on the kinetics of shale oil coking as a function of substrate type and temperature using gasified, combusted, and pyrolyzed shales. In a similar manner, the current study will focus on product adsorption and cracking. However, unlike the coking study which utilized freshly generated shale oil, the measurement of adsorption and cracking kinetics in the system described here dictated the use of model compounds.

Experimental. Reactor System. A simplified schematic of the reactor system is shown in Figure 1. High purity N₂ is introduced to a heated valve oven (275 °C) at 100 psig, split into parallel carrier lines and routed through a pair of metering valves. From the metering valves to the reactor, all carrier/transfer lines are constructed of 1/16" x 0.03" 304 ss.

One of the carrier lines, termed the bypass line, is routed through a switching valve, an 18" heat traced transfer line, a 48" preheater coil, and into one of the parallel tube reactors positioned in a 2"

x 15" Lindberg tube furnace. In the initial "bypass" mode, this line is routed through the substrate-packed reactor (substrate reactor).

High purity Ar is introduced at 100 psig and metered to the parallel HC carrier line just downstream from the N₂ metering valve. A Waters model 6000A LC pump is used to dispense the liquid hydrocarbon (HC) which first passes through a restriction coil to maintain pump back pressure (and thus constant flow), then into the valve oven where it passes through a downward spiraling volatilization/surge suppressor coil before connecting to the HC carrier line. The HC line parallels the bypass line to the reactor furnace where, in the initial valve position, it passes through the sand-packed bypass reactor.

After passing through the parallel reactors, both lines are combined and continuously sampled just inside the reactor furnace by a heated capillary connected to the inlet of a VG/Fisons Sensorlab 300D quadrupole mass spectrometer (QMS). The QMS may be operated in either a log histogram mode which monitors all mass intensities at 1-amu resolution from zero to a selected upper limit (usually just above the molecular ion of the model compound) or in a selected ion monitoring (SIM) mode which records up to 16 selected ion intensities at approximately 1 second intervals. The latter is the preferred operating mode due to a more rapid sampling rate but with the trade-off that not all ion intensities are monitored.

The tube reactors are constructed of 9" x 3/8" -o.d. (1/4" i.d.) 316 ss. One of the reactors, the bypass, is packed with 6-gm of sand while the second, the substrate reactor, is packed with 4-gm of one of the substrates listed in Table 1. Quartz wool is used to hold the solids in place. Substrates are centered in the reactor tubes with an approximate 2" void on each end. A type K thermocouple is placed into each reactor tube, 2.5" from the entrance to the bypass tube and 4" from the entry to the substrate tube. The substrate was removed following each run, crushed, and submitted for elemental analysis. The bypass sand was replaced after each 650 °C run (or when the model compound or study substrate was changed).

Study Substrates. The three substrates examined in this study (Table 1) originated from the CLE-003 master sample taken from Fleming County, Ky.¹⁻³ These materials represent the three types of solids present in the pyrolysis section of the KENTORT II reactor to which the vapor phase shale oil is exposed. All three substrates were prepared in a fluid-bed reactor using N₂, steam, or air as the fluidizing media (Table 1). All three substrates were screened to 20 x 60 mesh. The Ottawa sand was screened to 20 x 30 mesh.

Run Conditions and Procedure. A nominal model compound flow of either 0.1 or 0.2-mL/min was used for all runs. A total gas flow of 150 mL/min (ambient temperature) was maintained through each reactor. This flow was comprised solely of N₂ in the bypass line. For the HC carrier line, Ar tracer gas flow was set to 50 mL/min; the volume of the gas phase model compound was calculated assuming ideal gas behavior; and the cumulative flow adjusted to 150 mL/min with high purity N₂.

Run preparation entailed packing 4-gm of substrate to the substrate reactor and 6-gm of sand to the bypass reactor, setting the Lyndberg furnace controller to the target temperature with the reactors in place, and initiating carrier gas and model compound flow. QMS data collection was initiated following a minimum 2-minute equilibration at temperature. The substrate thermocouple reading was manually maintained within ±2 °C of the target temperature for the duration of the run. After a minimum of 100 data points were collected in the SIM mode (or at least 2 minutes in the log histogram mode), the valve was rotated so that the HC carrier passed through the substrate reactor (make-up line is simultaneously switched to the bypass reactor). Following the selected exposure time, the valve was returned to the initial position and the QMS baseline reestablished. Control runs were made by packing both the bypass and substrate reactor tubes with sand to ensure acceptable system operation.

Data Management. Following data collection, the QMS data files are imported to a spreadsheet where the model compound's molecular ion (and/or selected cracking product) intensity is ratioed to

the Ar intensity. These ratios are then exported to a curve-fitting software routine (Sigma Plot) where a linear equation was fitted to the data points collected in the bypass mode (before and after HC/substrate exposure). A function containing both linear and decaying exponential terms (eq. 1) was fitted to the molecular ion/Ar ratio obtained during substrate exposure:

$$\text{Eq. 1} \quad y = -a \cdot \exp(-bt) + c \cdot t + d$$

The difference in the integrated area between the linear and exponential equations over the substrate exposure interval represents either product loss due to cracking/coking reactions for the high temperature runs ($\sim 500^\circ\text{C}$), to HC adsorption for low temperature runs ($\sim 400^\circ\text{C}$), or to a combination of these at the mid temperature ($\sim 400\text{--}500^\circ\text{C}$). Further, since the HC flow is known, HC loss can be expressed on an absolute basis, i.e., gms HC/gm substrate.

RESULTS AND DISCUSSION: A typical run sequence in which cyclohexene was passed through gasified shale at 500°C is shown graphically in Figure 2a. The response as plotted shows the ion intensity for the molecular ion of cyclohexene ratioed to the Ar ion intensity. Data are displayed as ratios instead of absolute intensities in order to correct for changing conditions during a run, e.g., QMS drift, pressure fluctuations, etc. The first segment represents QMS response in the initial valve position (bypass mode) in which the model compound is flowing through the sand-packed bypass bed. The second segment shows QMS response with the valve switched so that the model compound passes through the substrate reactor. The third segment shows the return to bypass mode at which time the QMS baseline is reestablished.

There is no measurable desorption in the data of Figure 2a following return to bypass suggesting that all product loss is attributable to cracking or coking losses. Evidence that this loss is due in large part to cracking reactions can be found in Figure 2b, which shows a substantial increase in the mass 42 (largely propene) to mass 82 (cyclohexene) ratio during exposure.

The high initial HC loss followed by a gradual decline to constant response was characteristic of the high temperature runs (Figure 4). Generally, substrate reactivity followed the order of gasified > combusted \geq pyrolyzed. Also, cyclic aliphatics were found to be more susceptible to induced reaction than were straight chain aliphatics with aromatics generally exhibiting the greatest stability. As of this writing, carbon analysis of the substrates is incomplete and thus product loss due to coking versus cracking cannot yet be differentiated. However, it is believed that cracking reactions (i.e., thermal cleavage with little or no coke deposition) are much more prevalent for aliphatics (particularly cyclic aliphatics) than aromatics which more likely undergo a higher proportion of coking reactions in the initial interaction. To help differentiate between cracking and coking losses, future runs are planned in which the total product stream will be combusted with the resulting CO_2 and H_2O products monitored with the QMS. It is anticipated that this approach will unambiguously determine coking losses with cracking losses determined by difference.

Figure 3 shows a similar cyclohexene/Ar ion intensity plot at a lower temperature of 300°C . HC loss in this run is attributed solely to adsorption since 1) the QMS response during the bypass mode and the latter portion of the expose mode are equivalent and 2) the desorption curve following return to bypass is equal in magnitude to the HC loss observed in the initial stages of substrate exposure. Generally, adsorption capacity followed the order of gasified \gg combusted \geq pyrolyzed shale. Adsorption was so extensive for many of the low temperature gasified shale runs that QMS response dropped off-scale resulting in a delay in data collection of up to 2 minutes in some instances.

SUMMARY. The reactor system described in this manuscript provides a rapid means of measuring HC reaction kinetics. The system is flexible in that direct comparisons of solid substrate reactivities may be compared over a wide temperature range with a variety of hydrocarbons. Though

not discussed, fixed gases are also amenable to adsorption/desorption studies by this technique. Future plans include: 1) examination of the liquid products and ultimate analysis of the solid substrates following exposure in order to help elucidate reaction mechanisms and differentiate between predominantly cracking versus predominantly coking reactions and 2) examining mixtures of two or more hydrocarbons to determine differential adsorption/desorption kinetics.

Acknowledgments. The author gratefully acknowledge the work of D.McLean, G. Thomas, and M. Moore for analytical support and S. Carter for providing the oil shale substrates and for valuable discussions. This work was supported in part by the Morgantown Energy Tech. Ctr., USDOE, under Coop. Agreement DE-FC21-90MC27286 (such support does not constitute an endorsement by the USDOE of the views expressed in this manuscript).

1. Carter, S.D., Taulbee, D.N., Rubel, A.R., Abner, R.T., *Proc.: 1988 Eastern Oil Shale Symp.,IMMR88/101*, Inst. Min. & Minerals Res., Lexington, Ky., May., 1989, p. 333-340.
2. Carter, S.D., Robl, T.L., Rubel, A.M., and Taulbee, D.N., *Fuel*, 1990, 69, p 1124.
3. Taulbee, D.N. and Carter, S.D., *Proc.: ACS Div. of Fuel Chem. 37, #2*, Fuel Chem. Div of ACS, pub., San Francisco, CA, April, 1992, pp. 800-809.
4. Carter, S.D., and Taulbee, D.N., *Fuel*, 71, #12, 1992, 1421-26.

Table 1. Study Substrates. Substrates dry screened to 20X60 mesh.

<u>Substrate</u>	<u>Origin</u>	<u>Reactor Load (g)</u>	<u>Preparation/comment</u>
Pyrolyzed Shale	Cleveland oil shale	4-g	530C in N ₂ /10 min
Gasified Shale	Cleveland oil shale	4-g	800C in Steam/20 min
Combusted Shale	Cleveland oil shale	4-g	700C in air/10 min
Sand	Ottawa, Canada	6-g	20X30 mesh

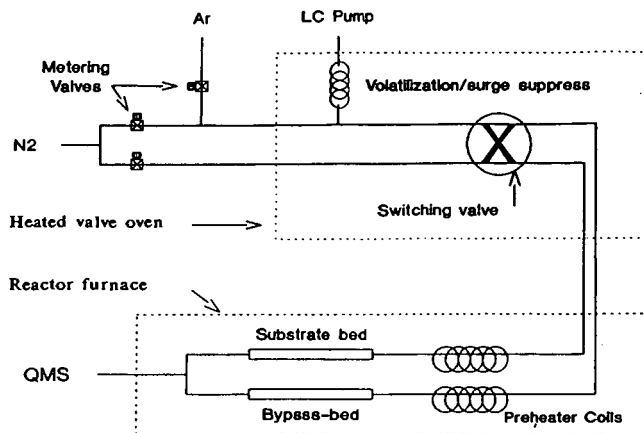


Figure 1. Adsorption/Cracking Reactor Schematic.

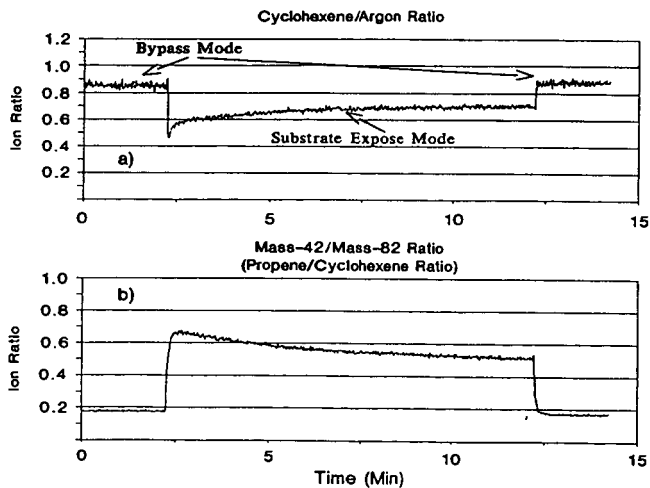


Figure 2. Gasified shale, 500 °C, 10 min exposure, ~10 vol% cyclohexene in Ar/N₂ carrier. a) Cyclohexene/Ar (82/20) ion ratios, b) Mass 42/mass 82 (largely propene).

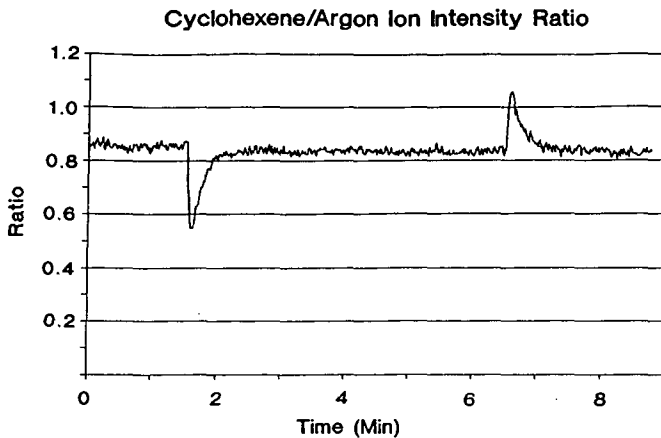


Figure 3. Cyclohexene/Ar ion intensity during gasified shale substrate run at 300 °C, 5 minute exposure. Otherwise, same conditions as Figure 2.

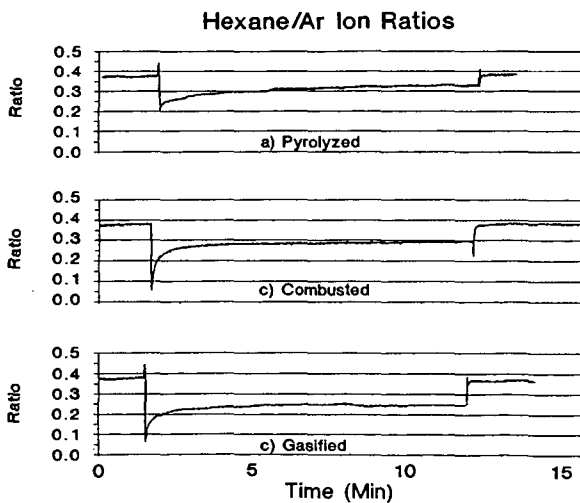


Figure 4. Hexane/Ar ion ratios for 650 °C, 10 min exposure runs, ~10 vol% hexane in Ar/N₂ carrier. a) pyrolyzed b) combusted and c) gasified substrate.

THE ROLE OF CATALYST PRECURSOR ANIONS IN CHAR REACTIVITY

Lillian L. Sims, Godfried M. K. Abotsi and Kofi B. Bota
Research Center for Science and Technology
Clark Atlanta University
Atlanta, GA 30314

Key words: Anions, zeta potential, metal adsorption

INTRODUCTION

Coal gasification activity is generally attributed to the metal components of catalyst precursors. However, there is evidence that the anion of the catalytic salt plays a significant role in the performance of the catalyst. It has been reported (1) that for the same metal, the chlorides, acetates, or hydroxides of sodium, potassium, magnesium, and calcium exhibited different char reactivities. The catalysts were loaded from aqueous solution. For example, at 1223K, the order of reactivity for the sodium compounds was $\text{NaOH} > \text{NaAc} > \text{NaCl}$. These findings were rationalized in terms of the influence of the various anions on the diffusivities of the cations (Na^+ , K^+ , Mg^{2+} , and Ca^{2+} produced by dissociation of the metal precursors at gasification temperatures) through the pores of the chars. The variations in the activities of the catalysts were also ascribed to differences in the extent of deactivation as a result of the catalyst reaction with inorganic materials in the coal, and to the presence or absence of coal surface metal-oxygen complexes which have been hypothesized as prerequisites for coal char reactivity (2-7). It has also been suggested that the metal ion of the catalyst salt reacts with the carbon in the char to form active intermediates for gasification and that the anion of the salt favorably modifies the structure of the active species. However, the composition and structure of the active intermediates are unknown (8).

Since coal is normally impregnated with catalyst from solution, the variations in the activities of different catalyst precursors may be due to the influence of different anions during the adsorption of the metal ions onto the coal. The surface charge properties of aqueous suspensions of coal is well known. The electrical potential on a coal particle decreases rapidly with distance from the charged coal surface. The effective thickness is the distance from the charged surface into the solution within which most of the electrical interactions with the surface occur (9,10). The effective thickness, $1/K$, (or the Debye length) is given by the expression (9, 10):

$$1/K = \left[(\epsilon_r RT) / (4\pi F^2 \sum_i C_i Z_i^2) \right]^{1/2} \quad (1)$$

where $\epsilon_r = \epsilon/\epsilon_0$ = the relative static permittivity or dielectric constant of the solution (ϵ = the static permittivity of the solution and ϵ_0 = the permittivity of a vacuum), R = the gas constant, T = the absolute temperature, F = the Faraday constant, C_i = the molar concentration of any ion in solution. The above equation shows that $1/K$ is inversely proportional to both the valence (Z) of the ions in solution and to the square root of their ionic concentrations. Also, in the presence of an electrolyte, the electrical effects are experienced over shorter distances (due to the compression of the electrical double layer) than in the absence of an electrolyte. Thus, the Debye length decreases rapidly with increasing ionic strength, given by $1/2\sum C_i Z_i^2$ (10).

In relation to catalyzed coal gasification, it is apparent from the above discussion that when different catalyst precursor electrolytes containing the same metal (e.g. KCl and K_2CO_3) are dissolved in aqueous solution and separately introduced into coal, the degree of coal-metal ion contact will be different for the various catalyst precursors due to differences in the double layer thickness. This will produce different metal adsorption densities and possibly different catalyst dispersion and gasification activities. Variations in catalyst uptake by coals can also occur as a result of differences in the pHs of the impregnating metal solutions. This work reports on the effects of catalyst precursor anions and pH on coal electrokinetic properties and catalyst adsorption by various calcium and potassium catalyst precursors.

EXPERIMENTAL

The surface electrokinetic properties of the raw coal (North Dakota Hagel lignite, PSOC 1482) in the presence or absence of acetate (CH_3COO^-), chloride (Cl^-), nitrate (NO_3^-), carbonate (CO_3^{2-}) or sulfate (SO_4^{2-}) anion was investigated by dispersing 300 mg of the coal (-200 mesh sieve size) in a liter of distilled water containing 10^{-1} , 10^{-2} or 10^{-3} mol/L of each anion. The potassium compound of each anion was used as the source of the anion while the acetate, chloride or nitrate of calcium was applied. The slurries were divided into 50.0 mL portions and the pHs were adjusted with a few drops of dilute nitric acid or ammonium hydroxide solution. The slurries were mechanically agitated for 3h to attain equilibrium followed by determination of the pHs and the zeta potentials using "Pen Kem model 501 Lazer Zee Meter."

The effects of the surface charge properties of the coal on the adsorption of potassium from CH_3COOK , KCl, KNO_3 , K_2CO_3 or K_2SO_4 solution has been ascertained by agitation (for 24h) of 4.0 g of the coal with 100 mL of solution containing 10^{-1} mol/L potassium metal. The catalyst precursors were used separately. Following the adsorptions, the coal particles were filtered and the potassium content in the coal samples was determined by Galbraith Laboratories, Inc.

RESULTS AND DISCUSSION

The effects of chloride anion concentration on the zeta potentials of the coal particles are shown in Figures 1 and 2, respectively, for $CaCl_2$ and KCl catalyst precursors. As can be observed from Figure 1, the charge density on the coal particles becomes progressively more negative, in the absence of added chloride anions, as the pH

of the slurry was raised from acidic to basic. However, addition of 10^{-2} or 10^{-3} mol/L chloride anion significantly reduced the net negative surface charge on the coal particles, especially at the higher chloride anion concentration. At \sim pH 10, for instance, the zeta potential of the coal is about -78 mV in the absence of chloride anion, but decreased to -15 and -40 mV, for the 10^{-2} and 10^{-3} mol/L Cl^- concentrations, respectively. Since the original coal particles are negatively charged, chloride anion adsorption will be hindered as a result of electrostatic repulsion between the coal surface and the chloride anion. Thus, the reduction in surface charge density must arise from the adsorption of calcium ions produced from the dissociation of calcium chloride, the driving force for the adsorption being coulombic attraction between the anionic coal surface and the calcium cations.

As in the case of the CaCl_2 precursor, Figure 2 shows that the zeta potentials of the coal particles decrease with increase in pH when KCl is used as the Cl^- source. It is also observed that, within experimental error, addition of KCl produces a less negative zeta potential compared to that on the coal without KCl addition. The development of surface charge on coal particles in aqueous media has been attributed to the dissociation of coal surface carboxylic and hydroxyl groups as discussed by several investigators (9,11-13). Comparison of Figures 1 and 2 shows that the reduction in the negative zeta potentials is more prominent, at similar chloride concentrations, for CaCl_2 than KCl. This behavior is consistent with equation (1) which predicts that the Debye length should be shorter in the presence of CaCl_2 than for KCl due to the higher ionic charge on Ca^{2+} compared to that on K^+ . This compression of the double layer promotes higher Ca^{2+} than K^+ uptake and results in a greater reduction in the net negative surface charge density in the presence of CaCl_2 . Similar trends were observed for the other corresponding calcium and potassium salts. To maintain a constant double layer thickness in studies involving interfacial phenomena, an excess of a 1:1 supporting electrolyte is normally added to the system. However, a supporting electrolyte was not applied in the current study in order to determine the influence of the various catalyst precursor anions or cations on coal surface chemistry.

The dependence of zeta potentials on pH and carbonate anion concentration, when using K_2CO_3 as CO_3^{2-} source, is provided in Figure 3. Similar zeta potentials were obtained in the presence or absence of CO_3^{2-} , particularly around \sim pH 2 - 4.5, for the 10^{-2} or 10^{-3} mol/L CO_3^{2-} concentration. However, significant reductions in the negative zeta potentials occurred at 10^{-1} mol/L CO_3^{2-} . The influence of the surface electrical properties of the coal on potassium adsorption from aqueous solutions of the potassium compounds is presented in Figure 4. The potassium uptake shows two distinct features: (1) a strong dependence on coal slurry pH, and (2) a dependence on the potassium salt used. For all the compounds, potassium adsorption was minimum around pH 2, it was maximum at \sim pH 10 and intermediate at pHs between 5 and 6. From Figure 4, it appears that at a given pH, the metal uptake can be classified into three groups according to the potassium precursor used: KCl, KNO_3 and K_2SO_4 fall into one group, while KOOCCCH_3 and K_2CO_3 belong to separate groups. It is evident from Figure 4 that the highest potassium loading was obtained at all pHs when adsorption was effected using potassium carbonate solution. The second highest metal uptake occurred when potassium acetate was used and approximately the same level of potassium was adsorbed from potassium chloride, potassium nitrate and potassium acetate solutions. As can be seen from Figure 3, the net negative surface charge density on the coal is significantly reduced in 10^{-1} mol/L CO_3^{2-} solution when K_2CO_3 was used as the carbonate anion precursor. The observed potassium loadings from this salt is in agreement with the zeta potential results. Thus, the surface charge on the coal clearly plays a role in potassium uptake. However,

the reasons for the variations in metal adsorption as a function of anion type are not known at this time and are the subjects of continuing research.

In conclusion, it has been shown that the negative charge density on a North Dakota lignite is reduced in the presence of CH_3COOK , KCl , KNO_3 , K_2CO_3 or K_2SO_4 solutions. For each compound, the reduction becomes more prominent as the salt concentration is increased, the phenomenon being particularly distinct for K_2CO_3 . Adsorption studies show that the highest potassium adsorption occurs from aqueous K_2CO_3 solution, thus confirming the zeta potential results which were least negative at 10^{-1} mol/L CO_3^{2-} when using K_2CO_3 salt. The reported superior activity of K_2CO_3 in char reactivity may reside in its stronger interaction with the coal surface during catalyst loading from solution. Fourier transform infrared studies are also in progress to gain insight into the interaction between the coal surface and the various ions.

ACKNOWLEDGEMENT

Financial support for this research was provided by the U. S. Department of Energy under contract number DE-FG22-91PC91286.

REFERENCES

1. Calahorro, C. V.; Gonzalez, C. F.; Garcia, A. B.; Serrano, V. G., *Fuel* 1987, 66, 216.
2. Wigmans, T.; Haringa, H., Moulijn, J. A., *Fuel* 1983, 62, 185.
3. Hashimoto, K.; Miura, K.; Xu, J. J.; Watanabe, A.; Masukami, H. *Fuel* 1986, 65, 489.
4. Wigmans, T.; van Craneburgh, H.; Elfring, R.; Moulijn, J. A., *Carbon* 1983, 21, 23.
5. Yuh, S. J.; Wolf, E. E., *Fuel* 1983, 62, 252.
6. Fredriks, I. L. C.; van Wechem, H. M. H.; Stuiiver, J. C. M.; Bouwman, R., *Fuel* 1981, 60, 463.
7. Mims, C. A.; Rose, K. D.; Melchior, M.-T.; Pabst, J. K., *J. Am. Chem. Soc.*, 1982, 104, 6886.
8. Wood, B. J. and Sancier, K. M. *Catal. Rev. Sci. Eng.* 1984, 26(2), 233.
9. Laskowski, J. S., Parfit, G. D., In "Interfacial Phenomena in Coal Technology," Botsaris, G. D. and Glazman, Y. M., Eds., Marcel Dekker, New York, 1988, p. 279.
10. Rosen, M. J., "Surfactants and Interfacial Phenomena," John Wiley, New York, 1978, p. 31.

11. Kelebek, S., Salman, T.; Smith, G. W., *Canad. Metal. Quart.* 1982, 21, 205.
12. Abotsi, G. M. K., Bota, K. B., Saha, G., *Energy & Fuels* 1992, 6, 779.
13. Fuerstenau, D. W.; Rosenbaum, J. M.; Laskowski, J., S., *Coll. Surf.* 1983, 8, 137.

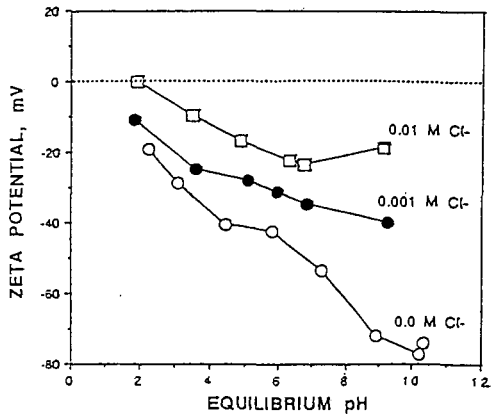


Figure 1. Dependence of zeta potential on the coal slurry pH and chloride anion concentration using CaCl_2 as the source of chloride. Coal: North Dakota lignite.

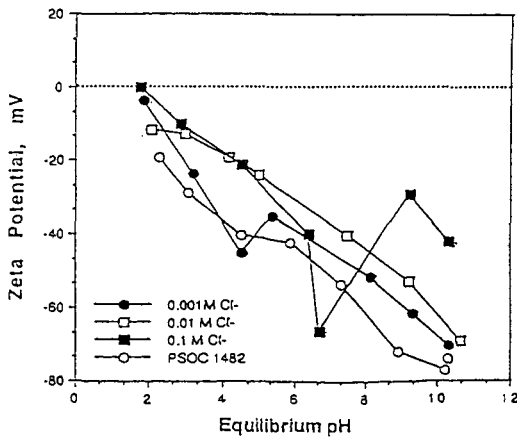


Figure 2. Dependence of the coal's zeta potential on pH and chloride anion concentration. KCl as source of chloride.

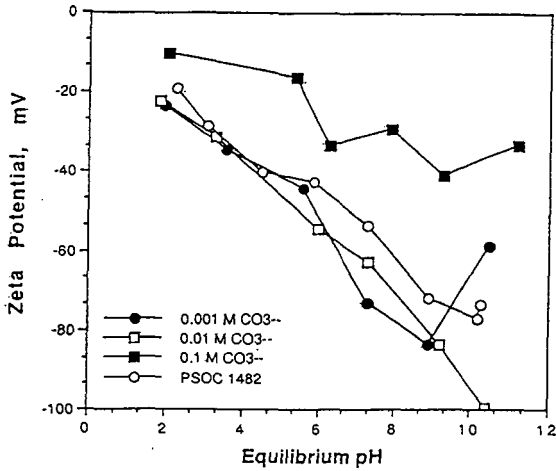


Figure 3. Variation of the coal's zeta potential with pH and carbonate anion concentration. K₂CO₃ as source of carbonate anion.

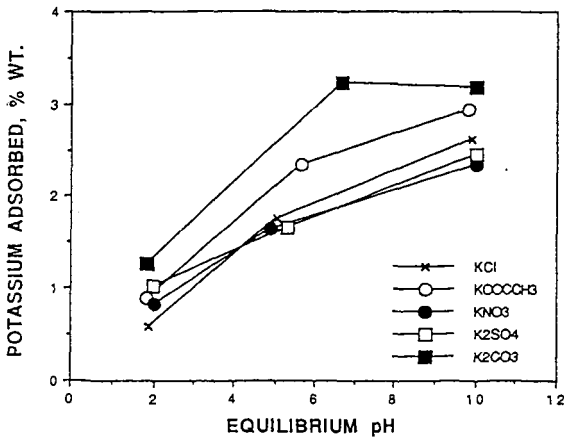


Figure 4. Influence of various potassium salts and pH on potassium adsorption by the coal.

Partial Oxidation of Ethane and Ethylene in the
Presence and Absence of ^{13}C Labeled Methane
on Reducible and Non-Reducible Oxide Catalysts

Abolghasem Shamsi
United States Department of Energy
Morgantown Energy Technology Center
P.O. Box 880
Morgantown, WV 26507-0880

Keywords: Catalysis; Oxidative coupling; Relative reactivity

INTRODUCTION

In recent years, there has been considerable progress in the development of catalysts for the conversion of natural gas to more useful chemicals and fuels. Oxidative coupling of methane to ethane and ethylene, and subsequent conversion of these chemicals to liquid fuel, is one approach that has attracted great interest in recent years (Liu et al., 1984; Yates and Zlotin, 1988; Otsuka et al., 1986). We have shown that by proper cation substitution in pervoskite-type oxides, active and selective catalysts for the oxidative coupling of methane to higher hydrocarbons can be obtained (France et al., 1988 (a and b); Shamsi and Zahir, 1989; Siriwardane and Shamsi, 1990). Recent studies have shown that gas-phase reactions, especially at higher pressures, play a significant role in the partial oxidation of methane (Labinger and Ott, 1987; Lane and Wolf, 1988; Shamsi and Zahir, 1989).

Despite intensive research on oxidative coupling of methane, no one has yet achieved a single pass yield large enough for a process to be economical. McCarty (1992) has evaluated several approaches for achieving higher yield in methane conversion processes. He has concluded that oxidative coupling of methane into desirable products is limited by two types of side reactions: "1) direct oxidation of reactive intermediates, and 2) the parallel conversion of desired metastable products into deep oxidation by-products."

Mazanec et al. (1992) studied methane conversion to higher hydrocarbons using electrocatalytic cells. They have concluded that "there is a fundamental mechanistic limitation to the conversion of methane to higher hydrocarbons." Olsbye et al. (1992) studied the effects of adding ethane and ethylene to an oxidative coupling reaction and found that methane is formed from the C_2 products. They suggested that the C_2 products are more reactive to form methane than the reverse methane coupling reaction. Mazanec et al. (1992) and Labinger (1992) have proposed a simple two-step "ABC" model. In this model, A is the reactants, B is the desired products, and C is the by-products. In this simplified model where

$$\text{A} \xrightarrow{k_1} \text{B} \xrightarrow{k_2} \text{C}, \text{ the } k_2/k_1 \text{ ratio is used to estimate the desired } \text{C}_2 \text{ yield.}$$

The challenging problem in converting methane to ethane and ethylene is the reactivity of methane relative to its products. There are at least three vital points in converting methane to ethane and ethylene using oxidative coupling. First, at high temperature and pressure, both homogeneous and heterogeneous reactions occur during oxidative coupling of methane, and the major precursors are produced in the gas phase (Shamsi and Zahir, 1989; Liu et al., 1984). Consequently, under these conditions it is difficult to change the product distribution entirely by tailoring the catalyst. Second, methane is much less reactive than its products, ethane and ethylene. Therefore, high conversion with high selectivity is very difficult to obtain. Third, complete oxidation of intermediates to carbon dioxide becomes increasingly important at higher pressure, which is required for a commercial process. The first and third problems could be overcome by developing a catalyst to activate methane at temperatures below 600°C and by designing a process that operates at 1 atm pressure. However, neither the catalyst nor the process design can solve the second problem. Ethane and ethylene, depending on their partial pressures, will compete for active species in the gas phase and for active centers on the catalyst surfaces as will be discussed later.

EXPERIMENTAL

See publication by Shamsi, A. and Zahir, K., (1989) for details.

RESULTS AND DISCUSSION

Earlier studies on oxidative coupling of methane indicated that the activation of methane occurs both in the gas phase and on the surfaces of the catalyst (Shamsi and Zahir, 1989). The results also showed that contact time, temperature, pressure, and methane-to-oxygen ratio are the major factors affecting conversion and selectivity in the presence and absence of the catalyst. Before investigating the catalytic oxidation, the effects of pressure, temperature, and contact time on partial oxidation of ethane and ethylene in an empty reactor were studied. This will determine the extent of gas-phase contribution to the overall reactions at various experimental conditions.

Ethane was partially oxidized by co-feeding ethane, helium, and oxygen into the reactor. The dependence of conversion and selectivity on temperature, pressure, and contact time is shown in Tables 1, 2, and 3. Ethane oxidation commenced at temperatures higher than 550°C. Higher ethane and oxygen conversions were obtained at higher temperatures, pressures, and contact times. Ethylene is the major product at low ethane conversion, and its concentration decreased with increasing temperature, pressure, and contact time. The amounts of CO and CO₂, carbon monoxide being predominant, also increased with increasing conversion. Methane, higher hydrocarbons, and formaldehyde were also detected at higher temperatures, pressures, and contact times, indicating that ethylene further reacts with oxygen to form formaldehyde and carbon oxides.

Ethylene was mixed with helium and oxygen and co-feed into the reactor. The dependence of conversion and selectivity on temperature, pressure, and contact time is shown in Tables 4, 5, and 6. Ethylene oxidation commences at temperatures higher than 500°C, about 50°C lower than required for ethane activation. Higher ethylene and oxygen conver-

sions were observed at higher temperatures, pressures, and contact times. Furthermore, at low ethylene conversion, ethylene oxide and formaldehyde are the major products, and their concentrations decreased with increasing conversion. The amount of CO increased with increasing conversion. This indicates that formaldehyde and ethylene oxide underwent further reactions to form carbon monoxide. Methane and higher hydrocarbons were also detected at higher temperatures, pressures, and contact times. Comparison with ethane shows that ethylene in an empty reactor, mainly gas-phase reactions, is oxidized more easily than ethane. These results are in good agreement with those reported by Burch and Tsang (1990). However, they have reported neither formaldehyde nor ethylene oxide.

Temperature-programmed partial oxidation of ethane, ethylene, and ^{13}C labeled methane was studied separately. Results are shown in Figures 1. The temperature was raised from 400 to 700°C at 40°C/min. Abundance of $^{12}\text{CO}_2$, $^{13}\text{CO}_2$, and oxygen were monitored using a GC with an MSD. The temperature at which 50% of the oxygen converted during oxidation of ethane and ethylene is significantly less than the temperature at which 50% of the oxygen converted during oxidation of methane. The rates of activation of these hydrocarbons on sodium promoted Sm_2O_3 decrease in the order of ethane > ethylene >> methane. Using these results and those in the literature to compare the reactivity of ethane and ethylene with methane would be misleading. According to the results shown in this graph, ethane and ethylene are activated at significantly lower temperatures than that required for methane activation. Therefore, any ethane or ethylene formed during oxidative coupling of methane would be consumed before any methane could be activated. The earlier results in this laboratory and elsewhere showed that this is not correct. Therefore, the relative reactivity of ethane and ethylene are different in the presence of methane and the catalyst as will be discussed later.

A mixture of ethylene in ^{13}C labeled methane were co-fed with oxygen and helium into the reactor (total flow rate of 17.5 cm³/min; hydrocarbon:oxygen ratio=2:1) containing 0.5 grams of 1.4 wt% sodium promoted Sm_2O_3 . The temperature of the catalyst bed was raised from 400 to 700°C at 40°C/min and held for 7.5 min at 720°C. The abundance (concentration, a.u.) of $^{12}\text{CO}_2$ and $^{13}\text{CO}_2$ was monitored using GC with an MSD. The concentrations of ethylene varied from 5 to 50 vol%. When the ethylene concentration was about 5 vol%, $^{13}\text{CO}_2$ was slightly more abundant than $^{12}\text{CO}_2$. However, increasing the concentrations of ethylene to 10 and 50 vol% formed more CO_2 from ethylene than from methane. No significant amount of carbon dioxide was detected at temperatures of less than 400°C and ethylene concentration of less than 10 vol%. However, when the concentration increased to more than 10 vol%, ethylene was activated at temperatures less than 400°C.

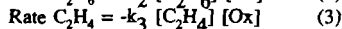
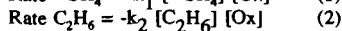
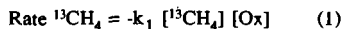
A plot of $^{12}\text{CO}_2$ to $^{13}\text{CO}_2$ ratios versus ethylene concentrations is shown in Figure 2. These data were obtained at steady state conditions of 720°C and 1 atm pressure. At a lower ethylene concentration of 5 vol%, ethylene was 7.8 times more reactive than methane. However, as the concentrations of ethylene increased to 10 and 50 vol%, the reactivity of ethylene decreased to 7.5 and 3.6, respectively. The relative reactivity was calculated based on the assumption that at equal reactivity and replacing 5, 10, and 50 vol% of ^{13}C labeled methane by ^{12}C ethylene, the $^{12}\text{CO}_2$ to $^{13}\text{CO}_2$ ratios will increase to 0.105, 0.222, and 2.0,

respectively. In all cases, when a mixture of methane and ethylene partially oxidized over quartz or the catalyst, higher ratios of $^{12}\text{CO}_2$ to $^{13}\text{CO}_2$ were obtained.

Temperature-programmed partial oxidation of mixtures of ethane in ^{13}C labeled methane over 1.4 wt% sodium promoted Sm_2O_3 were also studied. The temperature of the catalyst bed was raised from 400 to 700°C at 40°C/min and held for 7.5 min at 730°C. The abundance of $^{12}\text{CO}_2$ and $^{13}\text{CO}_2$ was monitored using GC with an MSD. The concentrations of ethane varied from 5 to 50 vol%. When the ethane concentration was about 5 vol%, the $^{13}\text{CO}_2$ was slightly more abundant than the $^{12}\text{CO}_2$, indicating that more than two moles of methane were converted to carbon dioxide per one mole of ethane. Increasing the concentrations of ethane to 10 and 50 vol% formed more carbon dioxide from ethane than from methane.

A plot of $^{12}\text{CO}_2$ to $^{13}\text{CO}_2$ ratios versus ethane concentrations is shown in Figure 3. These data were obtained at steady state conditions of 730°C and 1 atm pressure. At a lower ethane concentration of 5 vol%, ethane was about 5.5 times more reactive than methane. However, as the concentrations of ethane increased to 10 and 50 vol%, the relative reactivity of ethane decreased to 4.7 and 3.5, respectively. Comparing with ethylene mixtures, ethane at concentrations less than 10 vol% is about 1.5 times less reactive than ethylene. However, at concentrations of more than 10 vol%, ethane and ethylene show a similar reactivity and were about 3.5 times more reactive than methane.

Mazanec et al.(1992) have proposed that at the relative rates of methane and ethylene activation, k_2/k_1 , in equations (1) and (2) determine the upper limit of C_2 yield, considering ethane can be converted to ethylene readily by "non-oxidative pyrolysis".



They have also reported that "ethylene is more stable than ethane and the rate of ethylene activation is considered to be the limiting feature." However, the results obtained by passing a mixture of methane (34.7%), ethane (19.4%), ethylene (13.1%), and oxygen (32.8%) over a catalyst containing reducible oxides of transition metals (Ca/Ni/K= 2:1:0.1) show that almost all the ethylene was consumed while the concentration of ethane was reduced to 13.3% at 600°C and 1 atm pressure. When this similar mixture was passed over quartz chips at the same conditions, the concentrations of methane and ethylene increased to 42.7 and 19.1%, respectively. Therefore, rate equation (3) was added to explain the relative reactivity of methane and ethylene as the ratio of k_3/k_1 .

CONCLUSION

This study was conducted to understand the relative reactivity of ethane and ethylene compared to methane and to determine whether a catalyst could be designed to overcome the limitation in yield required for an economical process to convert natural gas to liquid fuels.

The most widely acceptable mechanism for activation of methane appears to be the reaction of methane from the gas phase with surface oxygen, which abstracts hydrogen from methane to form methyl radicals (Ahmed and Moffat, 1990). The methyl radicals are released into the gas phase and form ethane. However, the reaction pathways for activation of ethane and ethylene are not well established. The relative H-abstraction rates for hydroxyl radicals in the gas phase for C_2H_6/CH_4 and C_2H_4/CH_4 are reported by McCarty (1992). From these data and suggestion from Lunsford that the C-H bond strength in ethylene is greater than methane, the relative gas-phase reactivity can be estimated to be in the order of $C_2H_6 > CH_4 > C_2H_4$. However, this order was not observed in this study, and it has been reported only for $LiCl/MnO_x$ catalyst (Burch and Tsang, 1990), indicating that the H-abstraction is not the only pathway for ethane and ethylene activation. Likewise, depending on the catalyst and the experimental conditions, C-C and C=C bonds are also attacked by the active centers on the catalyst and by the active species in the gas phase. Therefore, the relative reactivity of ethane and ethylene compared to methane appears to strongly depend on the partial pressures of reactants and the type of catalysts used.

The relative reactivities are in the order of ethylene > ethane >> methane for reactions in the gas phase and on the catalysts containing reducible oxides of transition metals such as Ca/Ni/K. However, this order changed to ethane > ethylene >> methane for a non-reducible catalyst such as sodium promoted Sm_2O_3 . Oxidation of ethane and ethylene in the presence of methane and catalyst show that methane and ethylene, depending on their partial pressures, compete for active centers, and neither formaldehyde nor ethylene oxide were detected in the presence of methane and the catalyst.

LITERATURE CITED

- Ahmed, S.; Moffat, J.B., *Journal of Catalysis* 1990, 125, 54.
Burch, R.; Tsang, S. C., *Applied Catalysis*, 1990, 65, 259.
France, J.E.; Shamsi, A.; Ahsan, M.Q.; Headley, L.C., *Energy Progress* 1988 (a), 8(4), 185.
France, J.E.; Shamsi, A.; Ahsan, M.Q., *Energy & Fuels* 1988(b), 2(2), 235.
Labinger, J. A.; Ott, K. C., *J. Phys. Chem.* 1987, 91(2), 682.
Labinger, J.A., *Preprints-Symposia* 1992, 37(1), 289. ACS, 5-10 April, San Francisco, CA.
Lane, G.; Wolf, E. E., *Journal of Catalysis* 1988, 113, 144.
Liu, H.-F.; Liu, K. Y.; Johnson, R. E.; Lunsford, J. H., *J. Am. Chem. Soc.* 1984, 106(4), 117.
Mazanec, T.J.; Cable, T. L.; Frye, J. G. Jr., *Preprints-Symposia* 1992, 37(1), 135, ACS, 5-10, April, San Francisco, CA.
McCarty, J. G., *Preprints-Symposia* 1992, 37(1), 153. ACS, 5-10 April, San Francisco, CA.
Otsuka, K.; Jinno, K.; Morikawa, A., *Journal of Catalysis* 1986, 100, 353.
Olsbye, U.; Desgrandchamps, G.; Jens, K.-J.; Kolboe, S., *Preprints-Symposia* 1992, 37(1), 180. ACS, 5-10 April, San Francisco, CA.
Pereira, P.; Lee, S.H.; Somorjai, G.A.; Heinemann, H., *Catalysis Letters* 1990, 6, 255.
Shamsi, A.; Zahir, K., *Energy & Fuels* 1989, 3(6), 727.
Siriwardane, R.V.; Shamsi, A., *Applied Catalysis* 1990, 60, 119.
Yates, D. J. C.; Zlotin, N.E., *Journal of Catalysis* 1988, 111, 317.

Table 1. Effect of Temperature on Ethane Conversion and Selectivity in an Empty Alumina Reactor at 1 atm Pressure, $C_2H_6/He/O_2=20/20/10$ cm³/min NPT Flow Rates, Contact Time = 2.4 s

	Temperature (°C)		
	550	580	610
Conversion, Mol%			
Ethane	2.1	23.1	58.6
Oxygen	1.4	26.4	99.3
Product Distribution, Carbon Mol%			
C ₂ H ₄	100	84.9	54.2
CH ₄	0.0	2.1	8.3
CO	0.0	7.3	26.3
CO ₂	0.0	0.6	1.2
C ₃ ⁺	0.0	2.9	7.4
HCHO	0.0	2.3	2.6

Table 2. Effect of Pressure on Ethane Conversion and Selectivity in an Empty Alumina Reactor at 550°C, $C_2H_6/He/O_2=20/20/10$ cm³/min NPT Flow Rates, Contact Time = 2.4 s

	Pressure (atm)		
	1.0	1.7	2.4
Conversion, Mol%			
Ethane	2.1	8.1	57.4
Oxygen	1.4	7.5	99.4
Product Distribution, Carbon Mol%			
C ₂ H ₄	100	92.5	49.8
CH ₄	0.0	1.2	10.2
CO	0.0	1.9	27.2
CO ₂	0.0	0.9	1.4
C ₃ ⁺	0.0	2.1	7.2
HCHO	0.0	1.5	4.3

Table 3. Effect of Contact Time on Ethane Conversion and Selectivity in an Empty Alumina Reactor at 550°C, 1 atm Pressure, $C_2H_6/He/O_2=20/20/10$ cm³/min NPT Flow Rates

	Contact Time (s)		
	2.4	4.8	9.6
Conversion, Mol%			
Ethane	2.1	10.9	47.8
Oxygen	1.4	11.5	99.3
Product Distribution, Carbon Mol%			
C ₂ H ₄	100	92.2	55.5
CH ₄	0.0	1.4	6.6
CO	0.0	3.3	23.9
CO ₂	0.0	0.3	1.3
C ₃ ⁺	0.0	0.0	8.3
HCHO	0.0	2.7	4.4

Table 4. Effect of Temperature on Ethylene Conversion and Selectivity in an Empty Alumina Reactor at 1 atm Pressure, $C_2H_4/He/O_2=20/20/10$ cm³/min NPT Flow Rates, Contact Time = 2.4 s

	Temperature (°C)			
	500	538	546	560
Conversion, Mol%				
Ethylene	2.1	10.0	14.0	46.9
Oxygen	3.0	19.7	30.2	96.4
Product Distribution, Carbon Mol%				
C ₂ H ₆	0.0	0.7	0.0	2.4
CH ₄	0.2	0.7	1.0	14.3
CO	15.8	39.4	46.2	70.5
CO ₂	3.8	2.2	2.3	4.4
C ₃ ⁺	2.2	5.9	5.8	2.6
HCHO	26.0	19.4	14.8	2.4
C ₂ H ₄ O	52.0	31.7	29.9	3.4

Table 5. Effect of Pressure on Ethylene Conversion and Selectivity in an Empty Alumina Reactor at 500°C, C₂H₄/He/O₂=20/20/10 cm³/min NPT Flow Rates, Contact Time = 2.4 s

	Pressure (atm)			
	1.0	1.7	2.4	3.0
Conversion, Mol%				
Ethylene	0.9	5.7	18.1	44.4
Oxygen	1.3	6.1	37.6	90.2
Product Distribution, Carbon Mol%				
C ₂ H ₆	0.0	0.0	0.3	2.7
CH ₄	0.2	0.0	0.5	16.4
CO	15.8	23.7	37.9	66.3
CO ₂	3.8	3.1	4.4	5.0
C ₃ ⁺	2.2	3.1	6.1	2.2
HCHO	26.0	22.3	14.6	3.6
C ₂ H ₄ O	52.0	47.8	36.1	3.6

Table 6. Effect of Contact Time on Ethylene Conversion and Selectivity in an Empty Alumina Reactor at 500°C, 1 atm Pressure, C₂H₄/He/O₂=20/20/10 cm³/min NPT Flow Rates

	Contact Time (s)			
	2.4	3.2	4.8	9.6
Conversion, Mol%				
Ethylene	4.2	5.3	7.8	21.1
Oxygen	2.7	4.7	10.6	51.0
Product Distribution, Carbon Mol%				
C ₂ H ₆	0.0	0.0	0.0	0.6
CH ₄	0.2	0.3	0.5	1.0
CO	15.8	24.6	31.2	46.0
CO ₂	3.8	2.4	2.5	3.3
C ₃ ⁺	2.2	2.8	4.1	5.7
HCHO	26.0	21.5	18.1	10.3
C ₂ H ₄ O	52.0	48.4	43.6	33.2

Figure 1. Temperature-Programmed Oxidation of Ethane, Ethylene and ^{13}C Labeled Methane Over Sodium Promoted Sm_2O_3

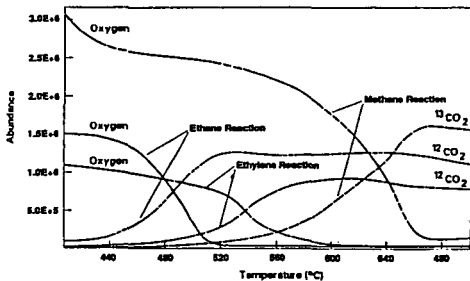


Figure 2. Effect of Ethylene Concentration in ^{13}C Labeled Methane on CO_2 Formation Over Sodium (1.4wt%) Promoted Sm_2O_3 at 725°C and 1 Atm Pressure

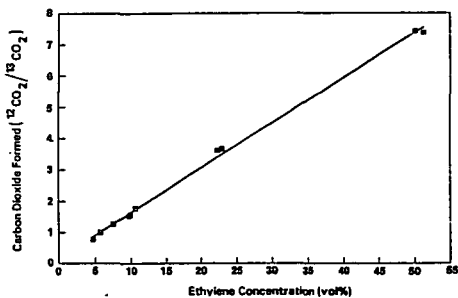
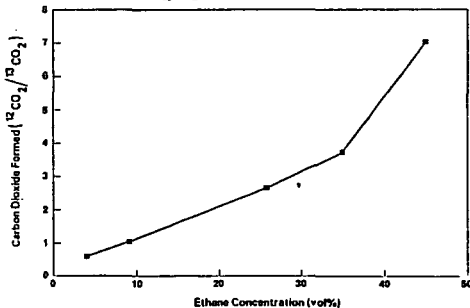


Figure 3. Effect of Ethane Concentration in ^{13}C Labeled Methane on CO_2 Formation Over Sodium (1.4wt%) Promoted Sm_2O_3 at 725°C and 1 Atm Pressure



PHOTODECOMPOSITION OF HYDRAZINE FUELS

Ghanshyam L. Vaghjiani
University of Dayton Research Institute
Phillips Laboratory, PL/RKFA
Edwards AFB, CA 92523

UV photometric measurement at 253.65 nm of hydrazine (N_2H_4) concentration in the gas phase has been used to study its 248.3-nm laser-photodissociation at 296 K. H-atoms, the major product in the photolysis, were directly detected by cw-resonance fluorescence. The primary quantum yield of $H(^2S)$ formation was measured to be 0.85 ± 0.15 . The reaction, $H + N_2H_4 \rightarrow \text{products}$; (k_1), that is initiated by the laser-flash was studied in the temperature range 296-222 K. The Arrhenius temperature dependence was determined to be $k_1 = (7.57 \pm 1.55) \times 10^{-12} \exp[-(1150 \pm 50)/T] \text{ cm}^3 \text{ molec}^{-1} \text{ s}^{-1}$.

INTRODUCTION

Hydrazine (N_2H_4), methylhydrazine (CH_3NNH_2), and unsymmetrical dimethylhydrazine ($(CH_3)_2NNH_2$), are an important class of nitrogen-based compounds that have positive standard enthalpies of formation. Decomposition of these compounds offer a wide variety of industrial applications such as in electrical power cells, fuels for thruster engines aboard the Space Shuttle and the Titan launch vehicles, as a mono-propellant, and in explosives. In addition to the above immediately practical reasons of studying hydrazine chemistry, the understanding of its laboratory photochemical decomposition is relevant to combustion because both processes can involve common reaction intermediates.¹⁻⁴ In this study we report the nature of the near ultraviolet absorption spectrum of N_2H_4 in the region 191-291 nm, the dissociation modes in the laser-photolysis at 248.3 nm, and the kinetics of the elementary reaction, $H + N_2H_4 \rightarrow \text{products}$, which is an important reaction in the pyrolysis of hydrazine fuels. Several previous studies on this reaction have all reported a different temperature dependence for this atom-molecule reaction. Our carefully chosen experimental conditions indicate that all but one previous study had interference from secondary reactions. Using our data and that of Stief and Payne⁵, it is now possible, for the first time, to make a recommendation for the Arrhenius activation energy and the pre-exponential factor for this reaction.

EXPERIMENTAL TECHNIQUE

The apparatus used to measure the ultraviolet absorption spectrum of N_2H_4 vapor is similar to that previously employed by Vaghjiani and Ravishankara,⁶ and the present experimental procedures are fully described elsewhere.⁷ The relative UV absorbance spectrum of a column of slowly flowing mixture of N_2H_4 /helium was monitored in a 100-cm-long Pyrex absorption cell using a diode-array spectrometer. The relative absorbance data was converted to absolute cross sections by using the 253.65 nm absorption cross section value determined in a separate experiment. In this experiment, as before, the 253.65 nm absorbance was monitored in a column of N_2H_4 /He, and the hydrazine

concentration in the experiment quantified by passing the eluting mixture through a series of Pyrex traps maintained at 77 K, and titrating the collected N_2H_4 with standard KIO_3 solution in 6 M HCl acid solution. The Beer-Lambert law, $A_{253.65} = \ell \sigma_{253.65} [N_2H_4]$, where $A_{253.65}$ is the measured absorbance at 253.65 nm, and ℓ the cell path length, was used to calculate the absorption cross section, $\sigma_{253.65}$, from the volumetrically determined hydrazine concentration, $[N_2H_4]$. The spectrum determined in this work together with data from previous work is shown in Figure 1.

The photodissociation of N_2H_4 was studied in a flash-photolysis apparatus of a design similar to that of *Vaghjiani and Ravishankara*.⁸ The formation of $H(2S)$ in the pulsed-laser photolysis (under optically thin conditions) of N_2H_4 was directly monitored by cw-resonance fluorescence detection of the ($2^2P^0 \rightarrow 1^2S$) transition in H-atoms at 121.6 nm. All experiments were carried out under slow-flow conditions, and under pseudo-first-order conditions in $[H]$ with the photolyte in an excess such that the temporal profile of $[H]_t$ immediately after photolysis followed an exponential relationship:

$$[H]_t = [H]_0 e^{-kt} \quad (1)$$

$[H]_t$ and $[H]_0$ are the concentrations of H-atoms at time t and zero, respectively. $k = k_1[N_2H_4] + k_d + \sum_i k_i[i]$, and is the pseudo-first-order rate coefficient for loss of $[H]$ in the gas mixture. k_1 is the second-order rate coefficient for the reaction $H + N_2H_4$, k_d is the first-order rate coefficient for diffusion of $[H]$ out of the detection zone, and k_i is the second-order rate coefficient for the reaction of H with minute impurities, i , in the gas mixture. Typical $[H]$ temporal profiles obtained are shown in Figure 2. The slopes of the decays give values for the pseudo-first-order rate coefficient, k , and the intercepts, S_{0N} (at time zero), a measure for the initial amount of H-atoms produced in the photolyses. The intercept in a given hydrazine photolysis is compared to the intercept, S_{0R} , obtained in a back-to-back photolysis of a known amount of CH_3SH under similar experimental conditions. The $[CH_3SH]$ is determined from the measured flow rates and the measured cell pressure. The $[N_2H_4]$ was directly determined by photometry at 253.65 nm. The observed initial signals, S_{0N} and S_{0R} need to be corrected for the attenuation of the detected 121.6 nm resonance fluorescence by the presence of the excess photolyte, and normalized by the photolytic energies, E_N and E_R , employed, respectively, in the two experiments.^{9,10} The plots in Figure 3 show how the observed signals, when normalized for the amount of photolyte present and photolysis energy employed, vary with the concentration employed. It can be shown that the primary $H(2S)$ quantum yield, Φ_N , in hydrazine photolysis is given by:

$$\Phi_N = \Phi_R \times \sigma_R / \sigma_N \times \exp(I_N) / \exp(I_R) \quad (2)$$

Φ_N , Φ_R , σ_N , σ_R , I_N , and I_R are the primary quantum yields for $H(2S)$ production, the absorption cross sections at 248.3 nm, and the intercepts in Figure 3, respectively, for each of the photolytes, N_2H_4 and CH_3SH . The values of the absorption cross sections used in this work are summarized in Table 1. Any revision in these values will directly affect the $H(2S)$ quantum yield computed in this study.

The kinetics of the reaction, $\text{H} + \text{N}_2\text{H}_4 \rightarrow \text{products}$; (k_1), was studied by measuring the pseudo-first-order rate coefficient, k , as a function of $[\text{N}_2\text{H}_4]$. A typical result at 296 K is shown in Figure 4. The straight line is a linear-least-squares fit to the data points whose slope yields a value for $k_1(296 \text{ K})$. k_1 was also measured at 273, 250, 232, 230, and 222 K.^{11,12} The Arrhenius temperature dependence of k_1 is shown in Figure 5. The straight line is a linear-least-squares fit to the data points. The temperature dependences obtained in previous studies are also shown in Figure 5.

RESULTS AND DISCUSSION

The absorption cross section at 253.65 nm, $\sigma_{253.65}$, was calculated to be $(2.86 \pm 0.17) \times 10^{-20} \text{ cm}^2 \text{ molec}^{-1}$ at 296 K. The normalized absorption spectrum in the region 191–291 nm is shown in Figure 1. The relative shape and the absolute values of this work and that of Biehl and Stuhl¹³ are in reasonable agreement to within $\pm 20\%$ in the wavelength region 195–230 nm. Becker and Welge's, discrete values in the vacuum-UV are also in good agreement.¹⁴ We are therefore confident that our photometric measurements at 253.65 nm give accurate absolute N_2H_4 number densities, to within $\pm 6\%$ (where the error is 1-sigma, precision plus systematic), in the photodissociation and kinetics experiments.

The continuous spectrum observed is indicative of absorption to one or more dissociative states. A variety of possible primary products can result on absorption of UV light.⁷ $\text{H} + \text{N}_2\text{H}_3$, $\text{NH}_2 + \text{NH}_2$, $\text{NH} + \text{NH}_3$, $\text{NH}_2(\tilde{\text{A}}^2\text{A}_1) + \text{NH}_2$, and $\text{N}_2\text{H}_2 + \text{H}_2$ can energetically form for photolysis wavelengths, λ , < 248.3 nm. We have measured directly, for the first time, an H-atom quantum yield, Φ_{H} , of 0.85 \pm 0.15 (where the error is 1-sigma, precision plus systematic) at 248.3 nm (Φ_{H} in CH_3SH is unity).¹⁵ The quantum yield was independent of laser fluences of up to $1.25 \text{ mJ cm}^{-2} \text{ pulse}^{-1}$ employed, and of the linear flow rate of the gas mixture ($2\text{--}8 \text{ cm s}^{-1}$) through the reaction zone. This indicates that 2-photon processes or subsequent photolyses of the reaction products formed in previous laser pulses, that may produce secondary H-atoms, is unimportant in our experiments. Our result is in excellent agreement with the indirect studies of Schurath and Schindler,¹⁶ who reported a yield of 0.97 ± 0.10 at 206.2 nm. Ramsay's,¹⁷ and Husain and Norrish's¹⁸ suggestion that $\text{NH} + \text{NH}_3$ and $\text{NH}_2 + \text{NH}_2$ are the major primary products in their flash-photolyses experiments is not consistent with our measured H-atom quantum yield. These latter intermediates are thought to be formed in subsequent secondary reactions after the initial flash. Within our experimental uncertainties, unit dissociation of hydrazine is suggested for absorption of 248.3 nm radiation due to a weak electronic transition to the lowest dissociative singlet, $\tilde{\text{A}}^1\text{A}$, state.

The Arrhenius temperature dependence of the reaction, $\text{H} + \text{N}_2\text{H}_4 \rightarrow \text{products}$; (k_1), is shown in Figure 5, and is given by $k_1 = (7.57 \pm 1.55) \times 10^{-12} \exp[-(1150 \pm 50)/T] \text{ cm}^3 \text{ molec}^{-1} \text{ s}^{-1}$. This is in excellent agreement with $(9.87 \pm 1.17) \times 10^{-12} \exp[-(1200 \pm 50)/T] \text{ cm}^3 \text{ molec}^{-1} \text{ s}^{-1}$ reported by Stief and Payne.⁵ However, the other three studies of Gehring et al.,¹⁹ Francis and Jones,²⁰ and Schiavello and Volpi²¹ all give different temperature dependences. These are also shown in Figure 5. The interference from secondary reactions at high radical concentrations, and or errors in estimating $[\text{N}_2\text{H}_4]$ employed in these later studies may be responsible for the differences in the reported values.

In this kinetic investigation of k_1 , we have minimized the importance of secondary chemistry by keeping $[\text{N}_2\text{H}_4]/[\text{H}]$ ratio high, typically 5×10^4 , and $[\text{H}]$ low, typically 1×10^{11} molec cm^{-3} , and have used excess He buffer gas to thermalize the initially produced translationally hot H-atoms in the photodissociation of N_2H_4 . Using our data and that of Stief and Payne,⁵ the recommended Arrhenius temperature dependence is derived to be $k_1 = (10.28 \pm 1.22) \times 10^{-12} \exp[-(1220 \pm 30)/T]$ $\text{cm}^3 \text{molec}^{-1} \text{s}^{-1}$. An activation energy of (2.4 ± 0.1) kcal mol^{-1} is obtained for this metathesis reaction in which the products are thought to be $\text{H}_2 + \text{N}_2\text{H}_3$.

We are currently looking at the temperature dependence of k_1 for $T > 296$ K, and the photodissociation of N_2H_4 at $\lambda < 248.3$ nm to get a through understanding of the dissociation mechanism(s) involved in hydrazine photolysis by UV light.

REFERENCES

- (1) Hepler, W. A.; Smith, O. I. *Symp. (Int.) Combust. Proc.* **1988**, *22*, 1799.
- (2) McHale, E. T.; Knox, B. E.; Palmer, H. B. *Symp. (Int.) Combust. Proc.* **1965**, *10*, 341.
- (3) Michel, K. W.; Wagner, H. Gg. *Symp. (Int.) Combust. Proc.* **1965**, *10*, 353.
- (4) Gray, P.; Lee, J. C.; Leach, H. A.; Taylor, D. C. *Symp. (Int.) Combust. Proc.* **6**, 255 (1956).
- (5) Stief, L. J.; Payne, W. A. *J. Chem. Phys.* **1976**, *64*, 4892.
- (6) Vaghjiani, G. L.; Ravishankara, A. R. *J. Geophys. Res.* **1989**, *94*, 3487.
- (7) Vaghjiani, G. L. *J. Chem. Phys.* **1993**, *98*, in press.
- (8) Vaghjiani, G. L.; Ravishankara, A. R. *J. Chem. Phys.* **1990**, *92*, 996.
- (9) Turnipseed, A. A.; Vaghjiani, G. L.; Gierczak, T.; Thompson, J. E.; Ravishankara, A. R. *J. Chem. Phys.* **1991**, *95*, 3244.
- (10) Talukdar, R. K.; Vaghjiani, G. L.; Ravishankara, A. R. *J. Chem. Phys.* **1992**, *96*, 8194.
- (11) Vaghjiani, G. L.; Ravishankara, A. R. *J. Phys. Chem.* **1989**, *93*, 7833.
- (12) Vaghjiani, G. L. *J. Phys. Chem.* **1993**, *97*, to be submitted.
- (13) Biehl, H.; Stuhl, F. J. *Photochem. Photobiol. A: Chem.* **1991**, *59*, 135.
- (14) Becker, Von K. H.; Welge, K. H. *Z. Naturforsch. Teil A* **1964**, *19*, 1006.
- (15) Wine, P. H.; Nicovich, J. M.; Hynes, A. J.; Well, J. R. *J. Phys. Chem.* **1986**, *90*, 4033.
- (16) Schurath, U.; Schindler, R. N. *J. Phys. Chem.* **1970**, *74*, 3188.
- (17) Ramsay, D. A. *J. Phys. Chem.* **1953**, *57*, 415.
- (18) Husain, D.; Norrish, R. G. W. *Proc. R. Soc. London, Ser. A* **1963**, *273*, 145.
- (19) Gehring, M.; Hoyeremann, K.; Wagner, H. Gg.; Wolfrum, J. *Ber. Bunsenges. Phys. Chem.* **1971**, *75*, 1287.
- (20) Francis, P. D.; Jones, A. R. *J. Chem. Phys.* **1971**, *54*, 5085.
- (21) Schiavello, M.; Volpi, G. G. *J. Chem. Phys.* **1962**, *37*, 1510.

Table I: Absorption cross section values used in this work
 $\sigma(10^{-20} \text{ cm}^2 \text{ molec}^{-1})$

λ (nm)	CH_3SH	N_2H_4
253.65	2.86
248.3	30.0	5.88

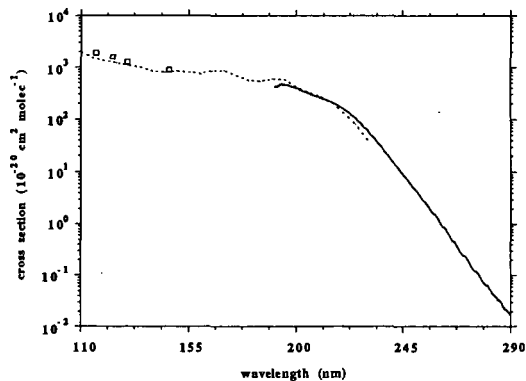


Figure 1. UV absorption cross sections of N_2H_4 . Solid line is this work, dashed line is from ref. 13, and squares are from ref. 14.

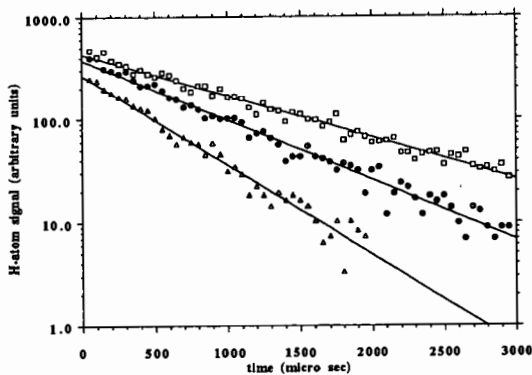


Figure 2. Typical [H] temporal profiles at 296 K. Each data point is the signal collected in 50- μ sec dwell-time and co-added over 5000 photolytic pulses. The slopes yield values for k and the intercepts values for S_{0N} .

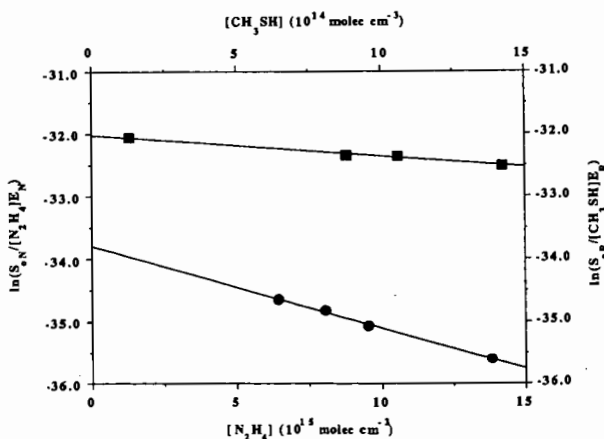


Figure 3. Variation of the log of normalized S_{0N} and S_{0R} signals with $[N_2H_4]$ (circles) and $[CH_3SH]$ (squares), respectively. Intercepts yield values for I_N and I_R , respectively, for the two photolytes.

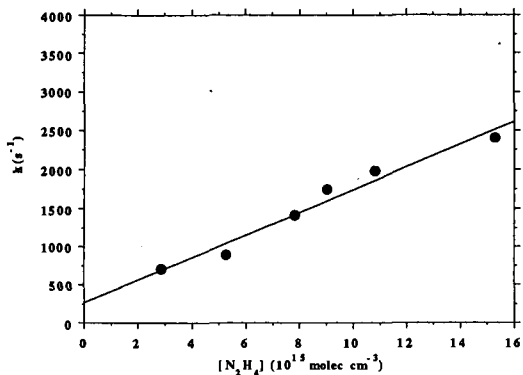


Figure 4. Plot of k versus $[N_2H_4]$. The slope yields a value for $k_1(296 \text{ K})$.

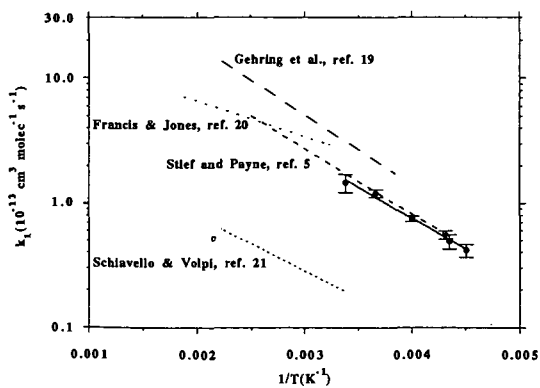


Figure 5. Arrhenius temperature dependences of k_1 . Data points are from this study.

POROUS γ -ALUMINA MEMBRANES MODIFIED WITH ULTRAFINE ZIRCONIA PARTICLES PREPARED BY REVERSED MICELLES METHOD

Katsuki Kusakabe, Takeyuki Yamaki, Hideaki Maeda and Shigeharu Morooka
Department of Chemical Science and Technology,
Kyushu University, Fukuoka 812 Japan

Keywords: Gas separation, Inorganic membrane, Reversed micelles

INTRODUCTION

Inorganic membranes have great potential as gas separation devices at elevated temperatures, but they have been little used to date. A major reason is that selectivity and permeability of inorganic membranes are not simultaneously achieved at an acceptable cost. If a high selectivity is requested in gas separation process, micropores in the membrane should be close to the size of gas molecules. This often reduces the permeability of that membrane. Porous inorganic membranes obtainable commercially have pore diameters ranging from 4 to 50 nm, where permselectivity is fundamentally controlled by Knudsen diffusion mechanism. Thus it is essential to develop a new membrane that shows an enough selectivity among small molecule gases without sacrificing the permeability.

In the present study, the outer surface of an α -alumina support membrane is coated with a thin layer of γ -alumina particles prepared by a sol-gel method. Further, micropores of the γ -alumina are narrowed with ultrafine ZrO_2 particles formed by a reversed micelles technique. The membrane obtained is evaluated with gas separation tests.

FORMATION OF ULTRAFINE ZIRCONIA PARTICLES

Zirconium tetrabutoxide ($Zr(OC_4H_9)_4$, Tri-chemicals) was used as zirconia source. The surfactant was dioleoyl phosphoric acid (DOLPA), which was synthesized according to the method of Goto et al. (1989). Water content in reversed micelles formed with DOLPA was decreased by two orders of magnitude when the pH value was decreased from 6 to 3.5 (Goto et al. 1990). This implies the reversed micelles can be destroyed by acidification.

Figure 1 shows the flow chart for the production of ultrafine zirconia particles by the reversed micelles technique. Ammonia and KCl was dissolved in a part of water to optimize ionic strength and pH. The same part of isooctane, in which DOLPA was dissolved, was placed on the top of the aqueous solution, and the aqueous phase was gently stirred at 303 K for 24 h. Stable reversed micelles were formed in the isooctane phase, which was recovered with a separation funnel. A butanol solution of zirconium tetrabutoxide was mixed to the isooctane solution. Zirconium tetrabutoxide was transferred to micro water pool in reversed micelles and then hydrolyzed to zirconia. After stirred at 303 K for 24 h, the reversed micelles were destroyed by adding an aqueous nitric acid solution, and finally the organic and aqueous phases were separated.

The concentration of zirconium in the aqueous phase was tried to determine with ICP-AES (SEIKO I. SPS-1200VR), but no zirconium was detected. It was also impossible to recover

zirconia particles into the aqueous solution by adding copper or nickel ions forming strong coordination bond with normal surfactants. The presence of zirconium in the organic phase, on the other hand, was confirmed by x-ray luminescence analysis. These results mean that ultrafine zirconia particles were stabilized in the organic phase with DOLPA molecules coordinated to hydroxyl group of zirconia.

The average size of water pools formed in the organic phase was 5 nm from the results of the dynamic laser scattering measurement (Photal DLS-7000). If one zirconia particle is formed in each micelle, the particle size, calculated from the number of micelles formed, is on the order of 0.1 nm. Since the zirconia concentration in the organic phase is as low as $3.0 \times 10^{-5} \text{ mol} \cdot \text{L}^{-1}$, the size of the particles formed in the reversed micelles is estimated to be less than 1 nm. This was assured from the observation of zirconia particles with a TEM (JOEL JEM-200CX).

PREPARATION OF COMPOSITE MEMBRANE

Porous α -alumina hollow fibers supplied by NOK Corp. were used as the support. The outer surface of the support was coated with a thin layer of γ -alumina by the following procedure: A boehmite (γ - AlOOH) sol was formed by adding aluminium isopropoxide into water and peptizing the suspension with hydrochloric acid (Yoldas, 1975). The concentration of the sol was $0.6 \text{ Al} \cdot \text{mol} \cdot \text{L}^{-1}$. The hollow fiber, whose lower end was closed, was dipped in the sol for several minutes, dried overnight in the atmosphere and heated to 1023 K at $50 \text{ K} \cdot \text{h}^{-1}$ in an air stream. This dipping-firing procedure was repeated 4 times.

The concept of modifying the γ -alumina membrane with zirconia particles is illustrated in Fig. 2. The γ -alumina-coated hollow fiber support, one end was plugged and the other was connected to a vacuum line, was dipped in the organic phase where zirconia particles were suspended. Ultrafine zirconia particles were trapped in the γ -alumina layer by suction for 1 h. The treated hollow fiber was heated at $50 \text{ K} \cdot \text{h}^{-1}$ and kept at 673 or 873 K in an air stream. This procedure was repeated 6 times.

GAS PERMEATION

Gas permeation experiments were performed at 373-673 K using hydrogen, nitrogen and methane. The unnecessary surface of the support fiber except for the test part was coated with a SiO_2 - B_2O_3 - Na_2O sealant. The permeating gas from the outside to the inside of the membrane was carried with argon. The flow rate was measured with a soap-film flow meter, and gas compositions were analyzed by gas chromatography. The total pressure in the both side of the membrane was kept at atmosphere pressure.

The gas permeability largely decreased with increasing number of dipping-firing cycle when the calcination was carried out at 673 K for 2 h. The membrane surface was grayish, and it was suspected that micropores were blocked with carbonaceous matters which were not removed at this temperature. Then the calcination temperature was raised to 873 K. As shown in Fig. 3, the gas permeability remained at about 5 % of that of the initial γ -alumina membrane after six repetitions of the dipping-firing cycle, and was still larger than that of Vycor glass membranes (Tsapatsis et al., 1991). From the observation of a fractured

section with an FE-SEM (Hitachi S-900), the thickness of the $ZrO_2/\gamma-Al_2O_3$ layer hardly changed after the six repetitions. The line analysis of Zr across the fractured surface indicates that most of ZrO_2 particles were collected in micropores of the γ -alumina layer. The top surface of the membrane was gradually smoothed by repeating the impregnation cycle.

Figure 4 shows the effect of the zirconium concentration, based on the volume of the organic phase, on the permeability after three or six repetitions of the dipping-firing cycle. The permeability decreased with increasing zirconium concentration in the range lower than $2 \times 10^{-5} \text{ mol}\cdot\text{L}^{-1}$. Smaller particles were packed more tightly in micropores, and the selectivity for hydrogen became large. In the present experiment, the separation factor of hydrogen to nitrogen was about 4.5 after the sixth impregnation cycle at a zirconia concentration of $1 \times 10^{-5} \text{ mol}\cdot\text{L}^{-1}$ as shown in **Fig.5**. The separation factor obtained exceeded the value of the γ -alumina membrane, 3.4. The gas permeability was independent of the pressure drop across the membrane and the permeation temperature.

CONCLUSION

Ultrafine zirconia particles were formed by hydrolysis of zirconium tetrabutoxide in reversed micelles with a novel surfactant, DOLPA. By repeating the dipping-firing cycle, micropores of a γ -alumina membrane were plugged with the zirconia particles. The permeability of the membrane was ca. 5 % of that of the initial γ -alumina membrane after the six repetition. The permselectivity of hydrogen to nitrogen was increased to 4.5 from the initial value 3.4. The membrane was stable at 673 K.

REFERENCES

1. Goto, M., Kondo, K and Nakashio, F. *J. Chem. Eng. Japan* 1989, **22**, 79.
2. Goto, M., Kondo, K and Nakashio, F. *J. Chem. Eng. Japan* 1990, **23**, 513.
3. Yoldas, B.E. *Am. Ceram. Soc. Bull.* 1975, **54**, 289.
4. Tsapatsis, M., Kim, S., Nam, S.W. and Gavalas, G. *Ind. Eng. Chem. Res.* 1991, **30**, 2152.

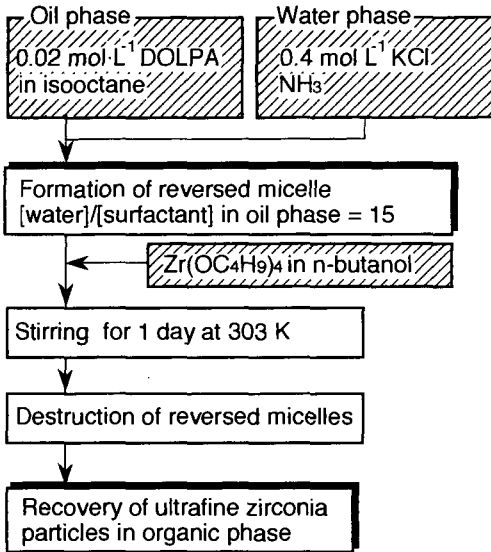


Fig. 1 Preparation of ultrafine zirconia particles by reversed micelles method

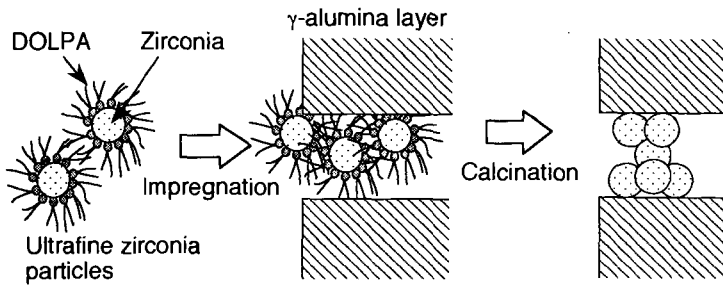


Fig.2 Preparation of zirconia/γ-alumina membrane

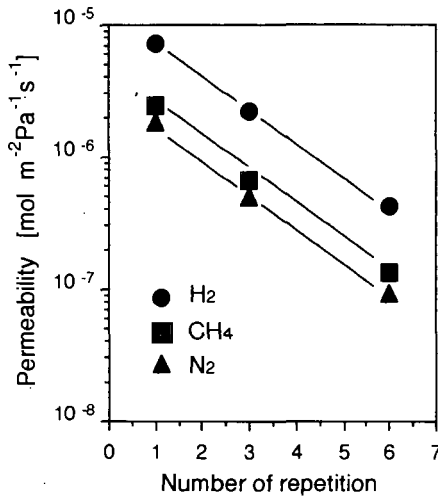


Fig. 3 Effect of repetition number of dipping-firing cycle on gas permeability. Permeation temperature = 373K, Zirconium concentration in organic phase = $1.0 \times 10^{-5} \text{ mol} \cdot \text{L}^{-1}$

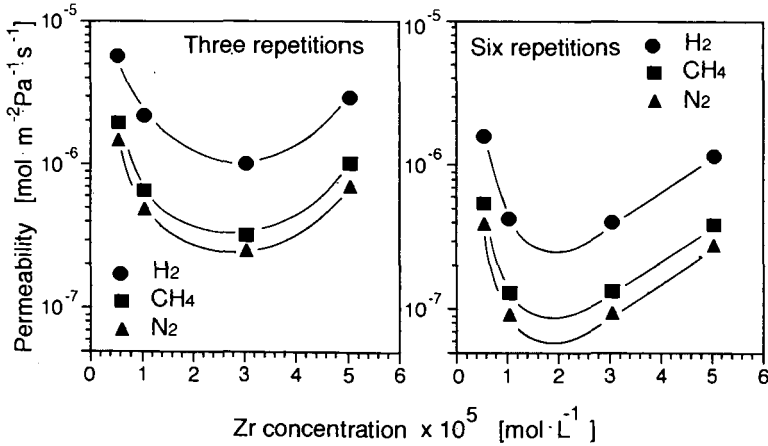


Fig. 4 Effect of zirconia concentration in organic phase on gas permeability. Permeation temperature = 373 K

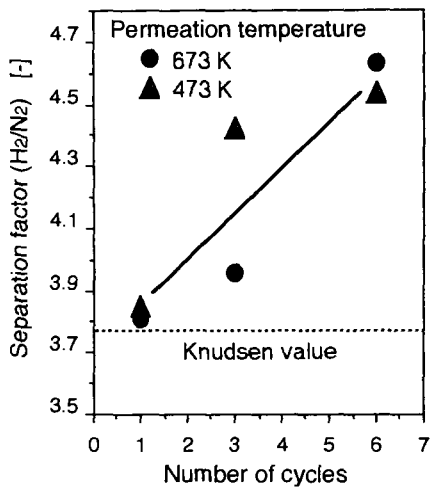


Fig. 5 Effect of repetition number of dipping-firing cycle on separation factor. Zirconium concentration in organic phase = $1.0 \times 10^{-5} \text{ mol} \cdot \text{L}^{-1}$